Development of novel multipotent compounds modulating endocannabinoid and dopaminergic systems

Development of novel multipotent compounds modulating endocannabinoid and dopaminergic systems

Alessandro Grillo,[a,1] Giulia Chemi,[a,1] Simone Brogi,[b] Margherita Brindisi,[c] Nicola Relitti,[a] Filomena Fezza,[d] Domenico Fazio,[e,f] Laura Castelletti,[g] Elisabetta Perdona,[g] Andrea Wong,[g] Stefania Lamponi,[a] Alessandra Pecorelli,[h] Mascia Benedusi,[i] Manuela Fantacci,[j] Massimo Valoti,[j] Giuseppe Valacchi,[h,i,k] Fabrizio Micheli,[g] Ettore Novellino,[c] Giuseppe Campiani,[a,] Stefania Butini,[a,]* Mauro Maccarrone,[f,l,2] Sandra Gemma[a,2]*

[1]These authors contributed equally to this work

[2]Equally senior authors

[a]*Department of Biotechnology, Chemistry and Pharmacy, DoE Department of Excellence 2018-2022, University of Siena, via Aldo Moro 2, 53100 Siena, Italy;* [b]*Department of Pharmacy, University of Pisa, via Bonanno 6, 56126, Pisa, Italy;* [c]*Department of Pharmacy, University of Napoli Federico II, DoE Department of Excellence 2018-2022, Via D. Montesano 49, 80131 Napoli, Italy;* [d]*Department of Experimental Medicine, University of Rome Tor Vergata, via Montpellier 1, 00133 Rome, Italy;* [e]*Faculty of Biosciences and Technology for Food Agriculture and Environment, University of Teramo, via R. Balzarini 1, 64100 Teramo, Italy;* [f]*Department of Medicine, Campus Bio-Medico University of Rome, Via Alvaro del Portillo 21, 00128 Rome, Italy;* [g]*Aptuit (Verona) Srl, an Evotec Company,* Via Alessandro Fleming, 4, 37135 Verona, *Italy;* [h]*NC State University, Plants for Human Health Institute, 600 Laureate Way, Kannapolis, NC 28081;* [i]*Department of Biomedical and Specialist Surgical Sciences, University of Ferrara, Via Borsari 46, 44121 Ferrara, Italy;* [j]*Department of Life Sciences, University of Siena, via Aldo Moro 2, 53100 Siena, Italy;* [k]*Department of Food and Nutrition, Kyung Hee University, Seoul, South Korea;* [l]*European Center for Brain Research, Santa Lucia Foundation IRCCS, Via del Fosso di Fiorano snc, 00176 Rome, Italy.*

KEYWORDS. Endocannabinoid system, fatty acid amide hydrolase, enzyme inhibitors, selective inhibitors, dopamine ligands, polypharmacology, multitarget compounds, dopamine receptor ligands

Corresponding Authors:

*Stefania Butini, Tel. +390577234161, email: butini3@unisi.it

**Giuseppe Campiani, Tel. +390577234172, email: campiani@unisi.it

[a]Abbreviations. AEA, anandamide; 2-AG, 2-arachidonoylglycerol; CBR, cannabinoid receptor; CB_1R, type-1 cannabinoid receptors; CB_2R, type-2 cannabinoid receptors; CNS, central nervous system; DCM, dichloromethane; DMF, dimethylformamide; DMSO, dimethylsulfoxide; eCBs, endocannabinoids; EDCI, 1-ethyl-3-(3-dimethylaminopropyl)carbodiimide; ECS, endocannabinoid system; FAAH, fatty acid amide hydrolase; *h*ERG, human ether-a-go-go related gene; HOBt, *N*-hydroxybenzotriazole; HPLC, high pressure liquid chromatography; MAGL, monoacylglycerol lipase; OS, Oxidative stress; PDB, Protein Data Bank; SAR, structure-activity relationship; TEA, triethylamine; THF, tetrahydrofuran.

Highlights

- Development of triple potent compounds as FAAH inhibitors and D_2/D_3 receptor ligands
- Structure-activity relationships were explored for the novel series of FAAH/D_2/D_3 ligands
- Cytotoxicity and mutagenicity tests were performed on selected compounds
- Preliminary metabolic studies were performed on compounds **3a** and **5c**
- Compounds **3a** and **5c** showed anti-inflammatory profile on IMR 32 cells

Abstract. Polypharmacology approaches may help the discovery of pharmacological tools for the study or the potential treatment of complex and multifactorial diseases as well as for addictions and also smoke cessation. In this frame, following our interest in the development of molecules able to modulate either the endocannabinoid or the dopaminergic system, and given the multiple and reciprocal interconnections between them, we decided to merge the pharmacophoric elements of some of our early leads for identifying new molecules as tools able to modulate both systems. We herein describe the synthesis and biological characterization of compounds **5a-j** inspired by the structure of our potent and selective fatty acid amide hydrolase (FAAH) inhibitors (**3a-c**) and ligands of dopamine D_2 or D_3 receptor subtypes (**4a,b**). Notably, the majority of the new molecules

showed a nanomolar potency of interaction with the targets of interest. The drug-likeliness of the developed compounds (**5a-j**) was investigated *in silico* while *h*ERG affinity, selectivity profile (for some proteins of the endocannabinoid system), cytotoxicity profiles (on fibroblast and astrocytes), and mutagenicity (Ames test) were experimentally determined. Metabolic studies also served to complement the preliminary drug-likeliness profiling for compounds **3a** and **5c**. Interestingly, after assessing the lack of toxicity for the neuroblastoma cell line (IMR 32), we demonstrated a potential anti-inflammatory profile for **3a** and **5c** in the same cell line.

1. Introduction

The endocannabinoid system (ECS) is the ensemble of fatty acid-derived messengers (endocannabinoids, eCBs), their receptors (type-1 and type-2 cannabinoid receptors, CB_1R and CB_2R), and the enzymatic machinery responsible for the biosynthesis and termination of the eCBs' signaling (in particular fatty acid amide hydrolase, FAAH, and monoacylglycerol lipase, MAGL).[1] The ECS plays a modulatory function in several physiological processes, mainly in the central nervous system (CNS). These effects are mostly operated via a retrograde signaling where post-synaptically released eCBs act at pre-synaptic CB_1R and modulate a series of functions (by the suppression of neurotransmitters' release).[2] The ECS is involved in several physiological (movement control, nociception, brain reward, learning and memory, feeding, brain development etc.) and pathological processes. By virtue of the interactions of the ECS with other neurotransmitter systems, the range of therapeutic options in which its modulation could be exploited is dramatically enlarged.[3] Among the various neurotransmitters of the CNS, the ECS has been frequently linked to dopamine.[4] In fact, the ECS operates indirect neuromodulatory effects on the dopaminergic system. This modulation is mediated by GABAergic and glutamatergic terminals "innervating" the dopaminergic neurons.[3] Increased or decreased of dopaminergic tone in the basal ganglia circuitry is associated with hypo- or hyper-motility, respectively.[5] In the basal ganglia circuitry the tight interconnection of ECS and dopaminergic system is also confirmed by

CB_1R and D_1 or D_2 receptors co-localization in striatal GABAergic projection neurons, and by the existence of CB_1R, D_2, and adenosine A_{2A} receptor heteromers in the dendritic spines of GABAergic neurons. Although the exact functional role of these heteromers needs to be further studied, their existence supports the presence of an eCB/dopamine bidirectional regulation.[3]

As regards the cortico-limbic structures, a "glitch" in the dopaminergic system is involved in psychoses such as schizophrenia as well as in addictive states.[3] In all these cases a normalization of the dopaminergic transmission is needed for attaining therapeutic efficacy. In light of the fact that cannabinoids are hypokinetic substances,[3] despite contrasting earlier reports,[6] more recent studies seem to indicate that a beneficial role for eCBs (such as anandamide, AEA) [7] in the modulation and prevention of the extrapyramidal symptoms elicited by D_2 antagonism could not be ruled out.

Further, the ECS signaling is also relevant in brain reward circuits and regulates the behaviors implied in addiction.[8] In this frame, a key level of interaction amongst ECS and dopaminergic system in mesocorticolimbic areas underlies processes like brain reward and drug abstinence responses. The fact that AEA plays a crucial role in the reward processes by activation of the dopaminergic system (in the mesolimbic area) is known since more than a decade.[9] Also, it has been demonstrated that FAAH inhibition contributes to this modulation, through potentiation of the AEA effects on dopaminergic neurotransmission.[9] The connection of the ECS to addiction substantiates its targeting also for the treatment of nicotine dependence, and in nicotine reward and relapse.[10, 11] In particular, FAAH inhibitors proved effective in reducing the anxiety induced by nicotine withdrawal.[12] This is a relevant issue for human health, since nicotine is the major psychoactive drug of tobacco, and tobacco use is associated with the death of 6 million people each year.[13]

As a further matter of fact, the mesolimbic pathway plays a key role in the control of emotions, and in reward. In particular, D_2-like receptor ligands, with a specific emphasis on D_3 receptor antagonists, have emerged as potential therapeutics for the management of abuse-related effects and

relapse of drugs of abuse.[14] Also some D_3 receptor antagonists have been engaged in clinical studies for smoking cessation and relapse prevention.[15] There are evidences indicating that D_2/D_3 receptor density may correlate with smoking and nicotine dependence. In a recent study in smokers and non-smoker subjects, by positron emission tomography, striatal dopamine D_2/D_3 receptor density was measured, and it was found that dopamine D_2/D_3 receptor availability was negatively correlated with recent and lifetime smoking and also with nicotine dependence.[16] This suggests that modulation of the D_2/D_3 receptor signaling may represent a potential treatment for nicotine addiction. In this context interesting achievements and prospects were recently reported through the development of FAAH/D_3 multiple ligands.[17, 18]

All these evidences converge to emphasize the high number of complex and multifactorial diseases and conditions that involve both the ECS and the dopaminergic system. The development of multitarget ligands for hitting both systems would be of note for a potential therapeutic application in different CNS diseases and cravings. In fact, a polypharmacological approach would offer the advantage of simultaneously targeting different neurotransmissional systems for attaining higher efficacy and lower toxicity than the administration of a cocktail of drugs.[19]

Since several years we have been deeply involved in the discovery of new CNS agents as potential therapeutics for schizophrenia,[20-22] and cocaine-seeking behavior.[23] The previously developed compounds belong to different structural classes, and the diverse scaffolds were strategically decorated for modulating their interaction with D_2 and D_3 receptor subtypes, and also with other monoaminergic receptors. More recently, we have reported the development of indirect agonists of the ECS (e.g. selective inhibitors of FAAH,[24-26] MAGL,[27] or dual FAAH/MAGL[28] inhibitors) and we have also studied different potential applications of FAAH-[29] and MAGL-targeting[30] pharmacological tools. In the context of a polypharmacological approach involving the ECS and the dopaminergic system, all the above considerations motivated us to give our contribution in the development of new FAAH/dopamine receptor modulators. Inspired by the structure of well-studied FAAH inhibitors bearing electrophilic centers (e.g.

carbamate) such as **1a**[31] and **1b**,[32] on the bis-aryl structure of **2**,[33] and based on our experience in the development of: i) FAAH potent reversible inhibitors (typified by **3a-c**,[24] Figure 1) ii) D_3 selective ligands (typified by **4a**,[23] Figure 1), and iii) multifunctional compounds for monoaminergic systems (typified by **4b**,[22] Figure 1), we merged the key pharmacophoric elements for the interaction with the targets of interest and we developed compounds **5a-j** (Figure 1 and Table 1) as potential dopaminergic D_2 and D_3 receptors ligands and FAAH enzyme inhibitors. The designed compounds bear an electrophilic functionality, needed for potent FAAH inhibition, and a phenylpiperazine moiety, a key feature for a potent D_2/D_3 interaction. These structures are supported on a versatile bis-aryl scaffold, where a phenyl system is linked to a 5-membered amidoheterocycle (Figure 1 and Table 1). Functionalization of this scaffold has enabled a systematic structure activity relationship (SAR) study.

We herein describe the synthesis, molecular modelling and biological investigation of compounds **5a-j**, which were tested on the FAAH enzyme and, for selected analogues, on D_2 and D_3 receptor subtypes. The drug-like profile and the physicochemical properties of the developed compounds were preliminarily assessed by computational methods. Their inhibition profile at human ether-à-go-go-Related Gene (*h*ERG) channels was calculated by our in-house 3D-QSAR model and for a subset of compounds the values were also experimentally determined. For compound **5a** and **5c** we assessed selectivity towards other ECS protein (CB_1R and CB_2R and MAGL enzyme). Cytotoxicity of compounds **5a** and **5c** was measured on mouse fibroblasts, and Ames test was performed to ascertain absence of mutagenicity. Preliminary metabolic stability studies were performed on **5c**, in comparison to **3a**, after incubation with human and rat liver microsomes in order to gain insights into potential metabolic stability issues. For compound **5c**, we demonstrated a potential antinflammatory profile on the neuroblastoma cell line (IMR32), by reducing the expression of the LPS-induced activation of the redox-sensitive transcription factor NF-κB.

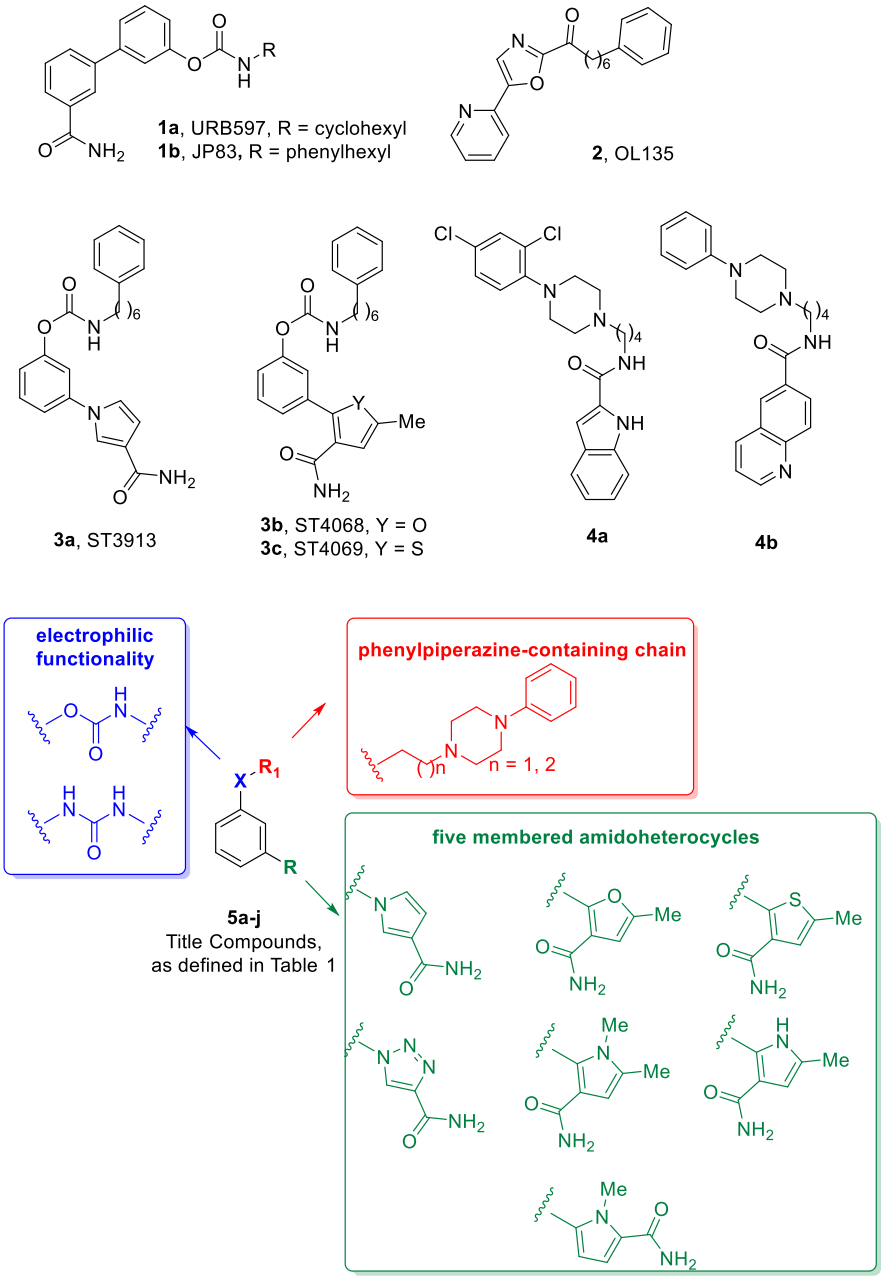

Figure 1. Reference (**1–4**) and title compounds (**5a–j**).

2. Results and Discussion

2.1. Chemistry

The synthesis of compounds **5a,b,i** is shown in Scheme 1. Amines **7a,b** were obtained following a literature procedure [34] encompassing alkylation of phenylpiperazine (**6**) with bromoacetonitrile or bromopropionitrile followed by reduction of the intermediate cyano derivative in the presence of lithium aluminium hydride. Carbonylimidazolide **8** was synthesized by treatment of amine **7a** with carbonyldiimidazole (CDI) in water. Known phenol derivative **9** [24], upon treatment with

phosgene in the presence of 4-(dimethylamino)pyridine (DMAP), afforded the corresponding chloroformate which was immediately reacted with amines **7a,b** providing final compounds **5a,i**, respectively. For the synthesis of the urea derivative **5b**, dimethoxytetrahydrofuran derivative **10** was submitted to Clauson Kaas reaction with 3-nitroaniline. Following reduction of the nitro functionality and partial hydrolysis of the nitrile to amide afforded key aniline derivative **11**. Treatment with phosgene followed by reaction with amine **7a** afforded derivative **5b**.

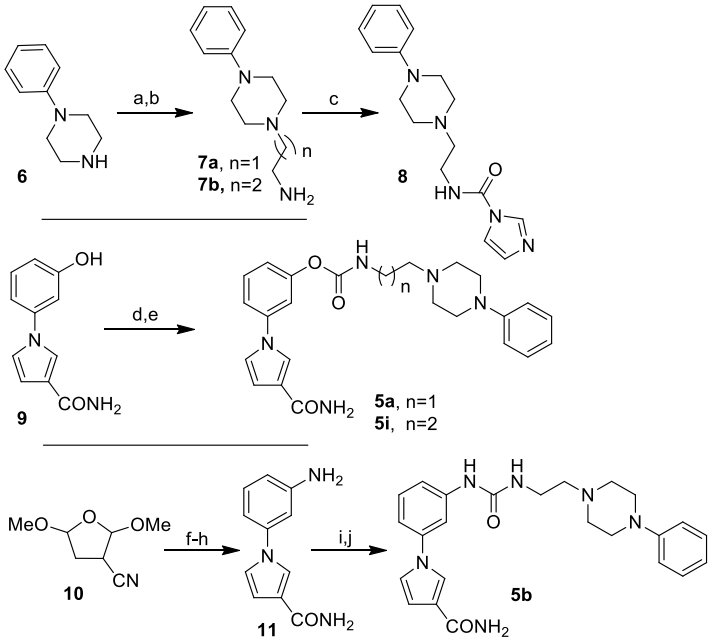

Scheme 1. Synthesis of compounds **5a,b,i.** Reagents and conditions. a) $BrCH_2CN$ or $BrCH_2CH_2CN$, Na_2CO_3, EtOH, 25 °C, 2 h, 65-70%; b) $LiAlH_4$, dry THF, 0 °C to 25 °C, 5 h, 50-60%; c) CDI, H_2O, 0 °C, 1 h, 90%; d) 20% $COCl_2$ in toluene, DMAP, dry THF, reflux, 12 h; e) **7a** or **7b**, dry THF, reflux, 12 h, 20% (over 2 steps); f) 3-nitroaniline, 6M HCl, 1,4-dioxane, reflux, 40 min, 92%; g) $SnCl_2 \cdot H_2O$, EtOH, reflux, 1.5 h, 95%; h) 6M NaOH, 30% H_2O_2, EtOH, reflux, 48 h, 32%; i) 20% $COCl_2$ in toluene, pyridine, dry DCM, 25 °C, 12 h; j) **7a**, dry THF, reflux, 12 h, 21% (over 2 steps).

The synthesis of phenylfuran- and phenylthiophene-based analogues **5c,d,j** is reported in Scheme 2. Reaction of known phenols **12a,b**[24] with phosgene in the presence of DMAP led to the chloroformate intermediates which after reaction with amines **7a,b** provided compounds **5c,d,j**.

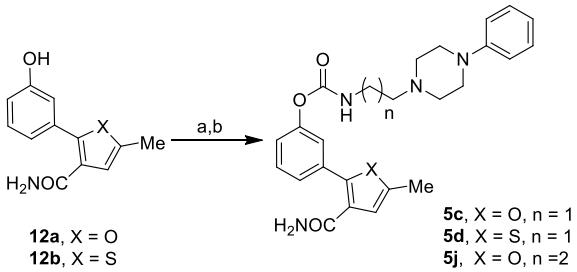

Scheme 2. Synthesis of compounds **5c,d,j.** Reagents and conditions. a) 20% $COCl_2$ in toluene, DMAP, THF, 0 °C to 25 °C, 30 min; b) amines **7a** or **7b** dry THF, reflux, 12 h, 30-34% (over 2 steps).

The synthesis of compounds **5e,f** is described in Scheme 3. Paal-Knorr reaction on dione **13** in the presence of methylamine and sulfamic acid as the catalyst[35] led to both the 2-aryl-1,5-dimethylpyrrolic derivative **15**, bearing the ester group in 3-position of the pyrrole ring, and its methylamide counterpart **14**. Ester **15** was hydrolysed to corresponding acid **16**, and converted into amide **17**, via classical coupling reaction with ammonium hydroxide in the presence of triethylamine (TEA), 1-ethyl-3-(3-dimethylaminopropyl)carbodiimide (EDCI), and hydroxybenzotriazole (HOBt). Amide **19** was directly obtained by reacting dione **13** with concentrated ammonium hydroxide in the presence of sulfamic acid. Also in this case, we observed the formation of both ester and amide derivatives **18** and **19**. The methoxyphenyl derivatives **17** and **19** were treated with boron tribromide to afford their phenolic counterparts **20a,b**. In this case, since classical reaction with phosgene and amine **7a** in presence of DMAP led to the isolation of the carbamoylated compound with a cyano group at 3-position of the pyrrole ring (deriving from amide dehydration), an alternative strategy involving reaction of phenol derivatives **20a,b** with carbonylimidazolide **8** was employed in order to obtain the compounds **5e,f**.

Scheme 4 describes the synthesis of compound **5g**. The commercially available pyrrole-2-carbaldehyde **21**, after protection as acetal derivative **22**, was brominated in 2-position (**23**) using *N*-bromosuccinimide (NBS). By treatment of **23** with 1M HCl acetal deprotection aldehyde **24** was obtained. Treatment of the aldehyde with iodine and ammonium hydroxide provided the cyano derivative **25** which was submitted to Suzuki coupling with 3-hydroxyphenylboronic acid to afford

phenol derivative **26**. Partial hydrolysis of the nitrile functionality let to amide derivative **27**. Treatment with phosgene followed by reaction with amine **7a** finally provided compound **5g**.

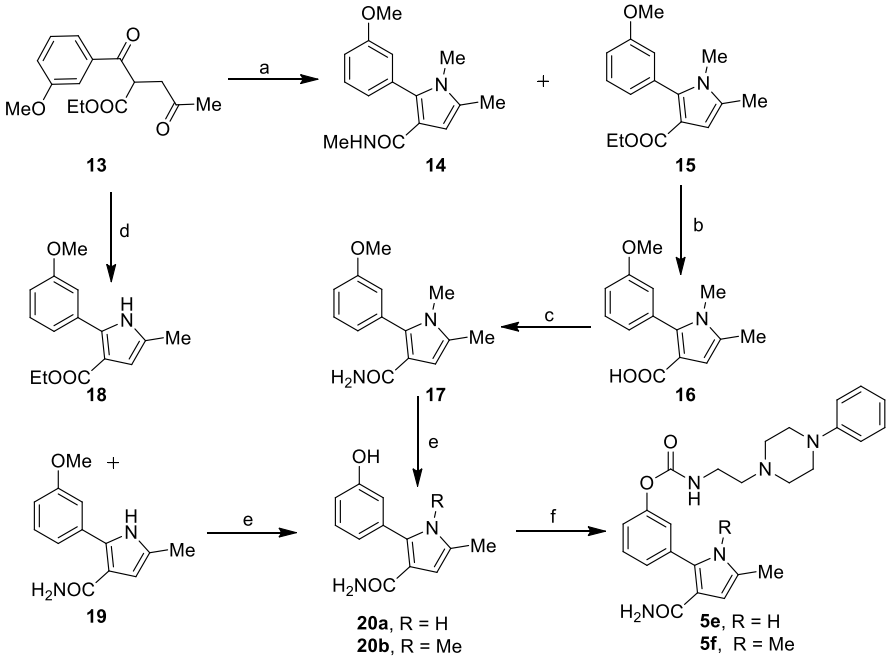

Scheme 3. Synthesis of compounds **5e,f.** Reagents and conditions. a) $MeNH_2$ (33% solution in EtOH), NH_2SO_3H, -5 °C to 25 °C, 2 h, 50%; b) NaOH, EtOH, H_2O, 65 °C, 16 h, 99%; c) TEA, EDC, HOBt, conc. NH_4OH, dry DCM, 0 °C to 25 °C, 16 h, 73%; d) Conc. NH_4OH, NH_2SO_3H, -5 °C to 25 °C, 5 h, 36% for **18**, 20% for **19**; e) BBr_3 (1M solution in DCM), dry DCM, -78 °C to 25 °C, 12 h, 20-22%; f), carbonylimidazolide **8**, H_2O, 25 °C, 5 h, 20-36%.

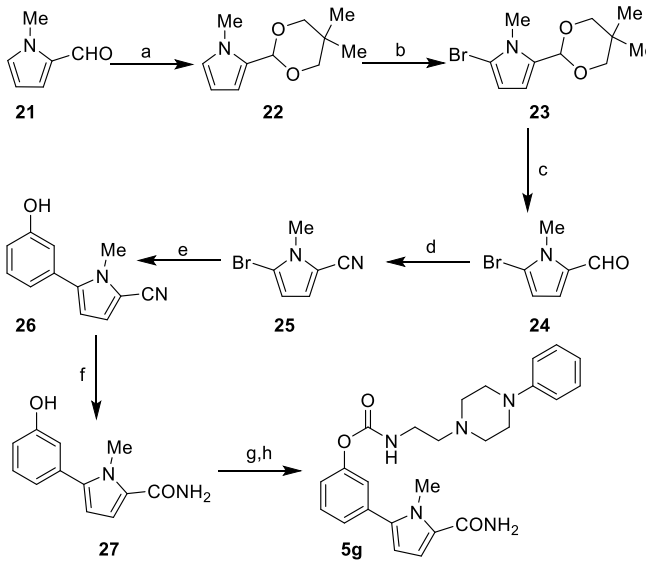

Scheme 4. Synthesis of compound **5g.** Reagents and conditions. a) *p*-Toluenesulfonic acid, 2,2-dimethyl-1,3-propanediol, toluene, 140 °C, 24 h, 99%; b) NBS, dry THF, -20 °C, 16 h, 81%; c) 1M HCl, acetone, 50 °C, 3 h, 83%; d) I_2, NH_4OH, THF, 25 °C, 16 h, 91%; e) 3-hydroxyphenylboronic acid, $Pd(PPh_3)_4$, Na_2CO_3/H_2O, EtOH, toluene, 25 °C for 10 min, then 80 °C for 3 h, 99%; f) 6M NaOH, 30% H_2O_2, EtOH, reflux, 48 h, 67%; g) 20% $COCl_2$ in toluene, DMAP, THF, 0 °C to 25 °C, 30 min; h) amine **7a**, dry THF, reflux, 12 h, 30% (over 2 steps).

The synthesis of derivative **5h** is described in Scheme 5. The commercially available 1-bromo-3-methoxybenzene **28** was converted into its corresponding azide **29**, by means of nucleophilic aromatic substitution, catalysed by copper(I) iodide (CuI) and *L*-proline.[36] The phenyltriazole **30** was then obtained by a conventional click chemistry reaction between **29** and methylpropiolate, in presence of CuI.[37] Saponification of the methyl ester, conversion of the acid **31** into the corresponding amide followed by the cleavage of the methoxy functionality, afforded phenol derivative **32**. Compound **32** was then converted, via the intermediate chloroformate, to the urethane **5h**.

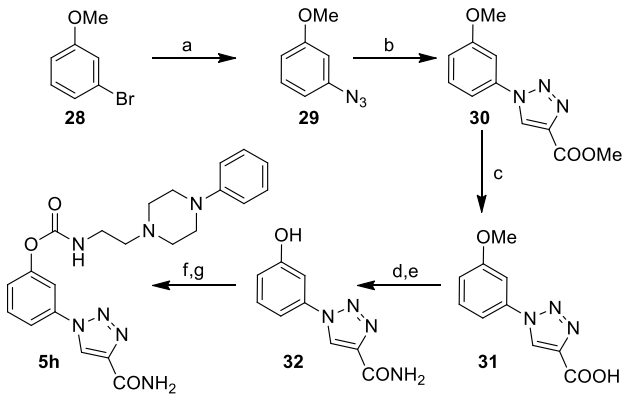

Scheme 5. Synthesis of compound **5h.** Reagents and conditions. a) NaN_3, CuI, *L*-proline, NaOH, H_2O, 95 °C, 16 h, 47%; b) methylpropiolate, CuI, DIPEA, dry THF, 25 °C, 12 h, 99%; c) NaOH, EtOH, H_2O, 65 °C, 16 h, 40%; d) *N*-methylmorpholine, isobutyl chloroformate, conc. NH_4OH, dry THF, -10 °C to 25 °C, 2 h, 99%; e) BBr_3 (1M solution in DCM), dry DCM, -78 °C to 25 °C, 12 h, 45%; f) 20% $COCl_2$ in toluene, DMAP, THF, 0 °C to 25 °C, 30 min; g) amine **7a**, dry THF, reflux, 12 h, 20% (over 2 steps).

2.2. Structure–activity relationship and molecular modeling studies

For the new compounds (**5a−j**, Table 1) the potency of inhibition of FAAH was assessed by means of inhibition studies, performed on the mouse brain enzyme, while affinity for D_2 and D_3 receptors was assessed by competition binding experiments performed on human recombinant receptors.

For gaining dopamine receptor affinity, the developed compounds **5a-j** were conceived by introducing a phenylpiperazine moiety, spaced by a 2 or 3 methylene bridge from the bis-aryl scaffold (phenyl linked to a 5-membered amido-heterocycle) which bears the reactive center (carbamate or urea) needed for the interaction with the FAAH enzyme. Inspired by the structures of

our previously developed FAAH inhibitors **3a-c** [24] with a sub-nanomolar potency (Figure 1 and Table 1) we observed that in the new series, the modifications introduced were well tolerated by the FAAH enzyme and most of the compounds were found to be potent FAAH inhibitors. The most interesting FAAH inhibitors were then selected for being tested against D_2 and D_3 receptor subtypes. In general, all the selected and tested compounds (**5a,c,d,h,i,j**, Table 1) displayed in vitro affinities for the dopamine receptors in the two or three digit nM concentration range.

In order to gain information about the possible binding modes of the tested compounds into the humanized variant of rat FAAH protein (*h*/*r*FAAH) binding site and in human D_2 and D_3 receptors, we performed a molecular docking calculation employing the Induced Fit Docking (IFD) technique as previously reported.[26, 28] The data were compared with those obtained for our lead **3a**.[24], [26] For each compound the physicochemical properties were calculated as well as their affinity for the *h*ERG K^+ channel.

Table 1. Inhibition Activity of compounds **5a-j** towards: Mouse Brain FAAH (as IC_{50} and K_i, nM) for Dopaminergic D_2 and D_3 receptors (as K_i, nM) and for *h*ERG channels (as IC_{50}, µM).

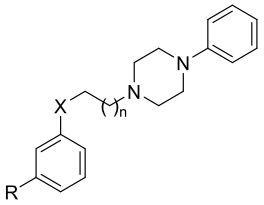

Cmpd	**R**	**X**	**n**	FAAH IC_{50} nM[a]	FAAH K_i nM[b]	D_2 K_i, nM (pK_i)[c]	D_3 K_i, nM [c] (pK_i)	*h*ERG IC_{50} µM[d] (pIC_{50})
1a	-	-	-	110 ± 23		NT	NT	NT
3a[24]	-	-	-	0.60[24]	0.16[24]	>30000 (<4.50)	>30000 (<4.50)	8.20 (5.10)
3b[24]	-	-	-	1.70[24]	0.49[24]	>30000 (<4.50)	>30000 (<4.50)	>10 (<5.00)
3c[24]	-	-	-	1.90[24]	0.50[24]	NT[e]	NT[e]	NT[e]
4a[23]	-	-	-	NT[e]	NT[e]	>10000[23]	0.18[23]	NT[e]
4b[22]	-	-	-	NT[e]	NT[e]	>1000[22]	0.60[22]	~10[22]
5a	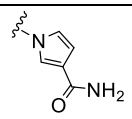	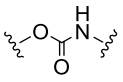	1	58 ± 12 (33-103)	16 ± 4.0	186 (6.73 ± 0.13)	105 (6.98 ± 0.05)	5.30 (5.28)
5b	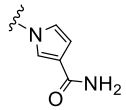	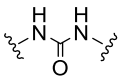	1	1600 ± 600 (1000-2500)	420 ± 100	NT[e]	NT[e]	NT[e]
5c	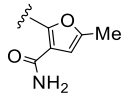	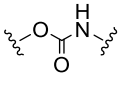	1	0.89 ± 0.11 (0.39-2.08)	0.23 ± 0.03	138 (6.86 ± 0.03)	105 (6.98 ± 0.11)	<0.10 (>7.00)
5d	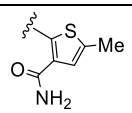	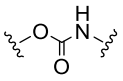	1	26.0 ± 1.30 (16.7-39.7)	6.88 ± 0.34	214 (6.67 ± 0.001)	148 (6.83 ± 0.01)	0.28 (6.55)
5e	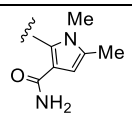	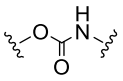	1	175 ± 40 (92-313)	46 ± 10	NT[e]	NT[e]	NT[e]
5f	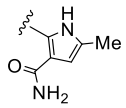	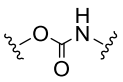	1	195 ± 25 (123-308)	50 ± 6.4	NT[e]	NT[e]	NT[e]
5g	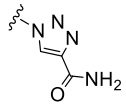	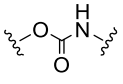	1	757 ± 60 (395-1450)	194 ± 15.4	NT[e]	NT[e]	NT[e]
5h	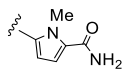	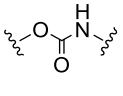	1	791 ± 25 (587-1066)	203 ± 6.30	56 (7.25 ± 0.06)	76 (7.12 ± 0.01)	6.40 (5.19)

5i	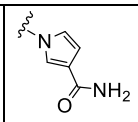	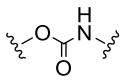	2	94 ± 18 (26.8-299)	25 ± 4.60	66 (7.18 ± 0.07)	34 (7.47 ± 0.07)	3.50 (5.45)
5j	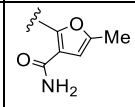	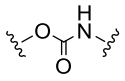	2	62 ± 6.70 (26.9-121)	16 ± 1.80	29 (7.53 ± 0.004)	19 (7.71 ± 0.05)	1.10 (5.97)

[a]Each value is the mean of at least three experiments (all SD are within 10%, 95 % confidence intervals are into brackets); [b]determined by the Cheng-Prusoff equation; [c](all SD are within 10%, pK_i values ± SD are into brackets); [d](pIC_{50} values are into brackets); [e]NT not tested.

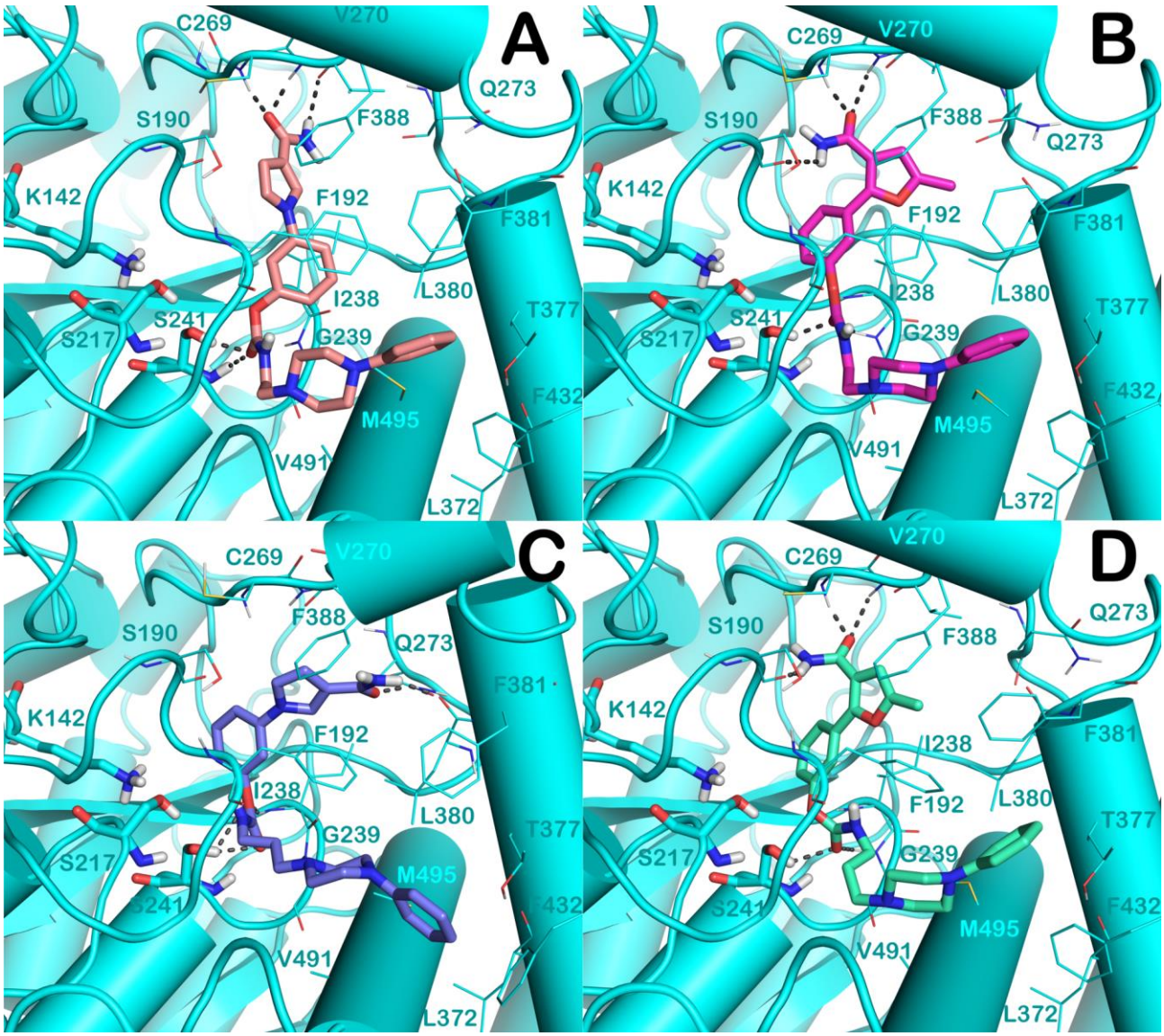

Figure 2. Binding modes of **5a** (light pink sticks in panel A), **5c** (magenta sticks in panel B), **5i** (light blue sticks in panel C), **5j** (light green sticks in panel D) into *h/r*FAAH enzyme (cyan cartoon, PDB ID: 3PPM) binding site. The residues forming the catalytic triad (K142, S217 and S241) are reported in sticks while the other residues of the binding site are reported as lines. The non-polar

hydrogens were removed for clarity. The pictures were generated by means of PyMOL (The PyMOL Molecular Graphics System, v1.8.4.0, Schrödinger LLC, New York, 2015).

The IFD protocol was able to confirm that the presence of an effective electrophilic center (such as the carbamate) was a key prerequisite for attaining high FAAH inhibition potency (Figures 2A-D and Figures S1A-F of the Supplementary Material). This moiety was indeed able, for most of the molecules of the set, to bind the catalytic S241, one of the three residues forming the catalytic triad (K142, S217, S241) and also to target one or more residues belonging to the oxyanion hole of the FAAH binding site (I238, G239, G240, S241) maintaining a conserved H-bond network. The modification of this moiety into an urea as in compound **5b** (Figure S1A) negatively affected binding mode and potency. In fact, although still in the nM range, the inhibition potency of **5b** (K_i = 450 nM) was 26 fold lower than that of the parent compound **5a** (K_i = 26 nM). In line with the drop of efficacy, **5b** was not able to target the catalytic residues, and formed alternative contacts (H-bonds, with M191, I238 and G239 located in front of the catalytic triad). For the other analogues we obtained a binding mode similar to that found for our previous potent FAAH inhibitors **3a-c**.[24], [26] Of note, compound **5c** (Figure 2B), the most potent inhibitor of the series, almost doubled the FAAH inhibition potency of its previously developed analogue **3b** (**5c** K_i = 0.23 nM *vs* **3b** K_i = 0.49 nM, Table 1). This data perfectly matched with the number of relevant contacts that **5c** established within the binding pocket. The carbamate formed a polar contact with S241, and an additional contact with G239. Other relevant contacts were also established by the methylfurancarboxamide moiety that, by its amidic portion formed polar contacts with the backbones of S190, C269 and V270. With this accommodation, the pendant phenyl ring of the phenylpiperazine system could interact, by a triple π-π stacking with F192, F381 and F432. Several SARs where explored by changing the nature of the 5-membered heterocycle. Modifying the furan into a thiophene (**5d**, Figure S1B) the tighter bond angle of the ring determined a different orientation of the molecule within the binding site, this event projected the amide in a different position where it could form only an H-bond with V270. The carbamate could establish H-bonds with S241 and I238, while the

phenyl stacked with F192. By modifying the ring with differently decorated pyrrole systems (with 1 or 2 methyl substituents) bound at different ring positions (**5a,e,f,h**) we observed a loss in the established contacts with a consequent loss of FAAH inhibition potency with respect to **5c**. For **5a** (Figure 2A) the pyrrol-1-yl junction and the presence of the amide moiety at 3-position, establishing polar contacts with C269 and V270, drove the specific accommodation of the molecule in the binding cleft where the phenyl system could stack with F192. Thus, the carbamate of **5a** formed two H-bonds with S241 (sidechain and backbone), whereas the aromatic portion of the phenylpiperazine system stacked with F381 and F432. Compounds **5e** and **5f** with a pyrrole-2-yl junction (Figure S1C and D) were able to enter in the gorge of the FAAH in a similar fashion to that of **5c**. They could interact with the S241 (by carbamate moieties) and with C269 and V270 (by the amide moieties), although establishing a lesser amount of contacts with respect to **5c**. In these compounds the methyl groups did not produce any relevant contact. For compounds **5g** and **5h** (Figure S1E and F), consistent with their lower FAAH inhibition potency, we found docked poses belonging to the most populated clusters that hampered the phenylpiperazine accommodation into the hydrophobic sub-pocket. The introduction of a triazole, as for **5g**, or of a 5-substituted pyrrole-2-yl portion (**5h**), did not improve inhibition potency, due to a lack of additional contacts besides that of the carbamate portion with S241. Notably, this latter interaction was less relevant as the interacting groups laid at a higher distance potentially precluding the nucleophilic attack. This observation is supported by the decrease of the inhibitory potency found for these compounds that were the weakest inhibitors of the carbamate series. The homologated analogues **5i** and **5j** (Figure 2C and D) displayed superimposable binding modes to that of the compounds **5a** and **5c**. As for the other analogues, also for **5i** and **5j** the carbamate drove the accommodation into the catalytic binding site although a slightly major distance between the carbamate and the catalytic Ser was observed. While compound **5j** (Figure 2D) retained the same accommodation of **5c**, for **5i** we found a different accommodation of the 3-amidopyrrole-1-yl portion (compared to **5a**) that interacts with Q273

(Figure 2C) due to the elongation of the aliphatic chain. Notably this residue was also targeted by our previously developed highly active compound **3a** as observed by us. [26]

Docking studies were also performed on the dopaminergic receptors. For improving the reliability of the *in silico* approach, we considered an implicit membrane model during the IFD (see experimental part for details). As reported in Figure 3A-F, we observed at the D_2 receptor a similar binding mode for the tested molecules. In particular, the phenylpiperazine portion of all the analyzed molecules (**5a,c,d,h,i,j**) was engaged in a series of interactions (π-π stacking or hydrophobic contacts) with the hydrophobic residues belonging to the seven trans-membrane (TMs) helices (TM1-7), identified as reported in Uniprot (Uniprot ID: P14416 (DRD_2_HUMAN) https://www.uniprot.org/uniprot/P14416) (V115 TM3, F198 TM5, F382 TM6, W386 TM7, F390 TM6). The carbamate portion of all the compounds could establish H-bonds with the key residue D114 (TM3) by its NH group and, for compounds **5a**, **5c** and **5i** (Figure 3A,B and E), polar contacts with Y408 (TM7) by their carbonyl group were observed. In general, the phenyl rings of the studied bis-aryl scaffolds established hydrophobic contacts with W100 and Y408. The amide moieties supported on the heterocycles contacted different D_2 receptor residues lining the extracellular site. In particular, **5a** (Figure 3A) established H-bonds with the sidechains of Y37 (on the surface of TM1) and T412 (TM7) and with the backbone of S409 (TM7). Compound **5c** is able to form an H-bond with the sidechain of E95 (TM2) (Figure 3B) as well as **5d** (Figure 3C). Compound **5h** interacts with the backbone of G98 (TM2) (Figure 3D). **5i** (Figure 3E) interacts by H-bonds with the sidechains of Y37 and E95, while **5j** with W100 (Figure 3F). Notably the mentioned binding modes with the key interactions in the TMs are similar to those observed for the crystallized ligand (Risperidone). All the discussed solutions showed a GlideScore < -10 kcal/mol in agreement with the nanomolar affinity of the compounds for the D_2 receptor.

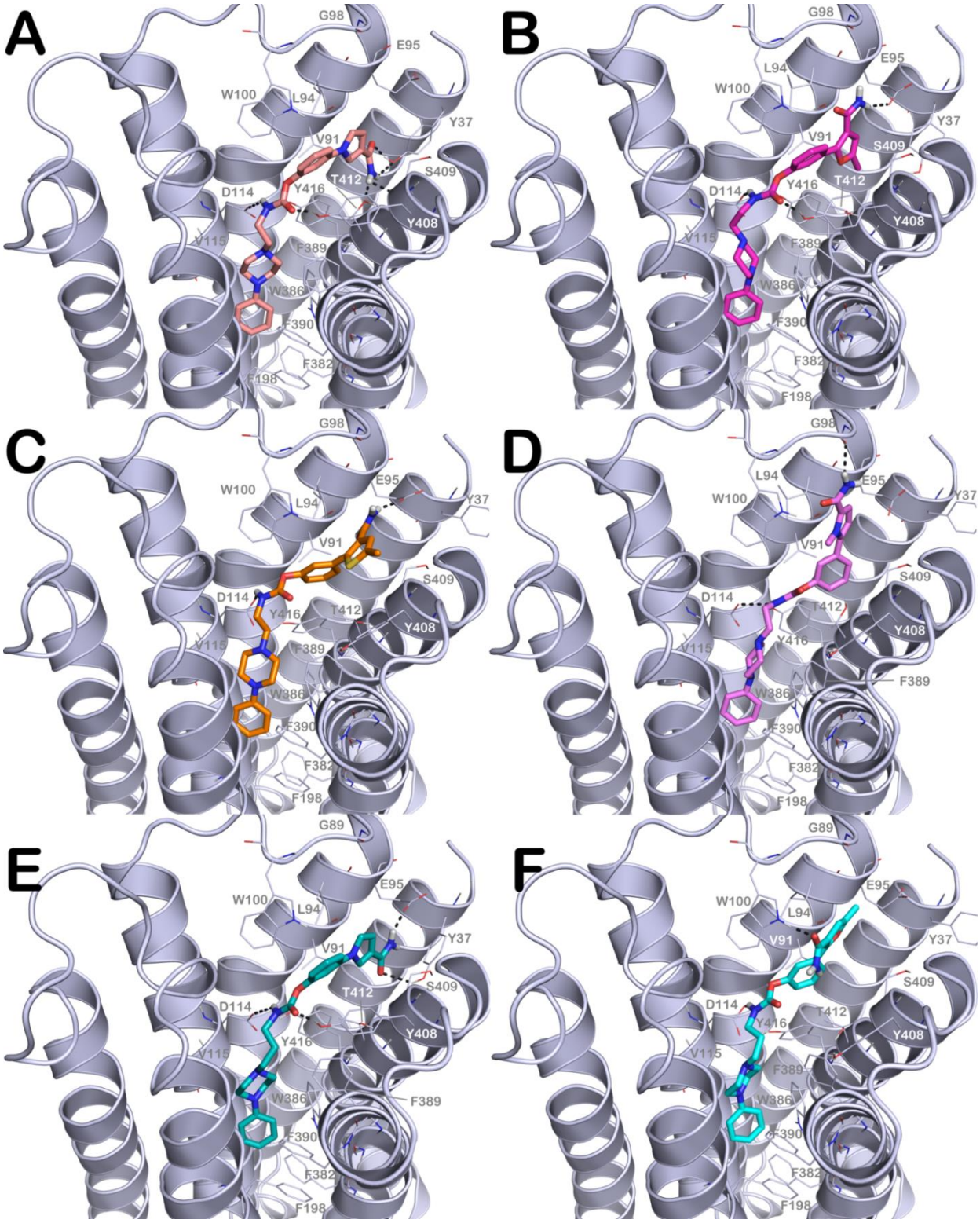

Figure 3. Binding modes of **5a** (light pink sticks in panel A), **5c** (magenta sticks in panel B), **5d** (orange sticks in panel C), **5h** (light magenta sticks in panel D), **5i** (dark green sticks in panel E) and **5j** (cyan sticks in panel F) into D_2 receptor binding site (grey cartoon, PDB ID: 6CM4). The residues forming the binding site are represented as lines. The non-polar hydrogens were removed

for clarity. The pictures were generated by means of PyMOL (The PyMOL Molecular Graphics System, v1.8.4.0, Schrödinger LLC, New York, 2015).

The studied compounds docked similarly also in the D_3 receptor binding site (Figure 4A-F) and showed a pattern of interaction in which the phenylpiperazine system was involved in hydrophobic interactions (π-π stacking or hydrophobic contacts) with the residues deeply located in TM3, TM5 and TM6 (V111 in TM3, V189 in TM5, F345, F346, H349, V350 in TM6). As already observed with the D_2 receptors, the NH group of the carbamate moiety could, for all the compounds, establish a H-bond with the key residue D110 on TM3, while the carbonyl group targeted different residues at TM7 such as Y365 (for **5a** and **5j**, Figure 4A and F), T369 (for **5c** and **5i**, Figure 4B and E) and S182 in TM5 (for **5h**, Figure 4D). The phenyl system of the bis-aryl moiety was engaged in hydrophobic interactions with Y36 (TM1) and V86 (TM2). The carboxamide moiety of **5a** strongly interacted with residues located at the surface of the D_3 receptor (Figure 4A). In particular, **5a** formed an H-bond with the sidechain of E90 (TM2). Compound **5c** (Figure 4B) stacked with Y365 by its furan ring. The same was verified for compound **5d** (Figure 4C), with the addition of an H-bond with the sidechain of H349. Compound **5h** (Figure 4D) interacted with the sidechain of T369. Compound **5i** formed H-bonds with the sidechains of S366 (TM7) and E90 (Figure 4E), while **5j** with the backbone of L89 (TM2) and the sidechain of E90 (Figure 4D). Also in this case the solutions showed a GlideScore < -10 kcal/mol in agreement with their nM affinity for the D_3 receptor.

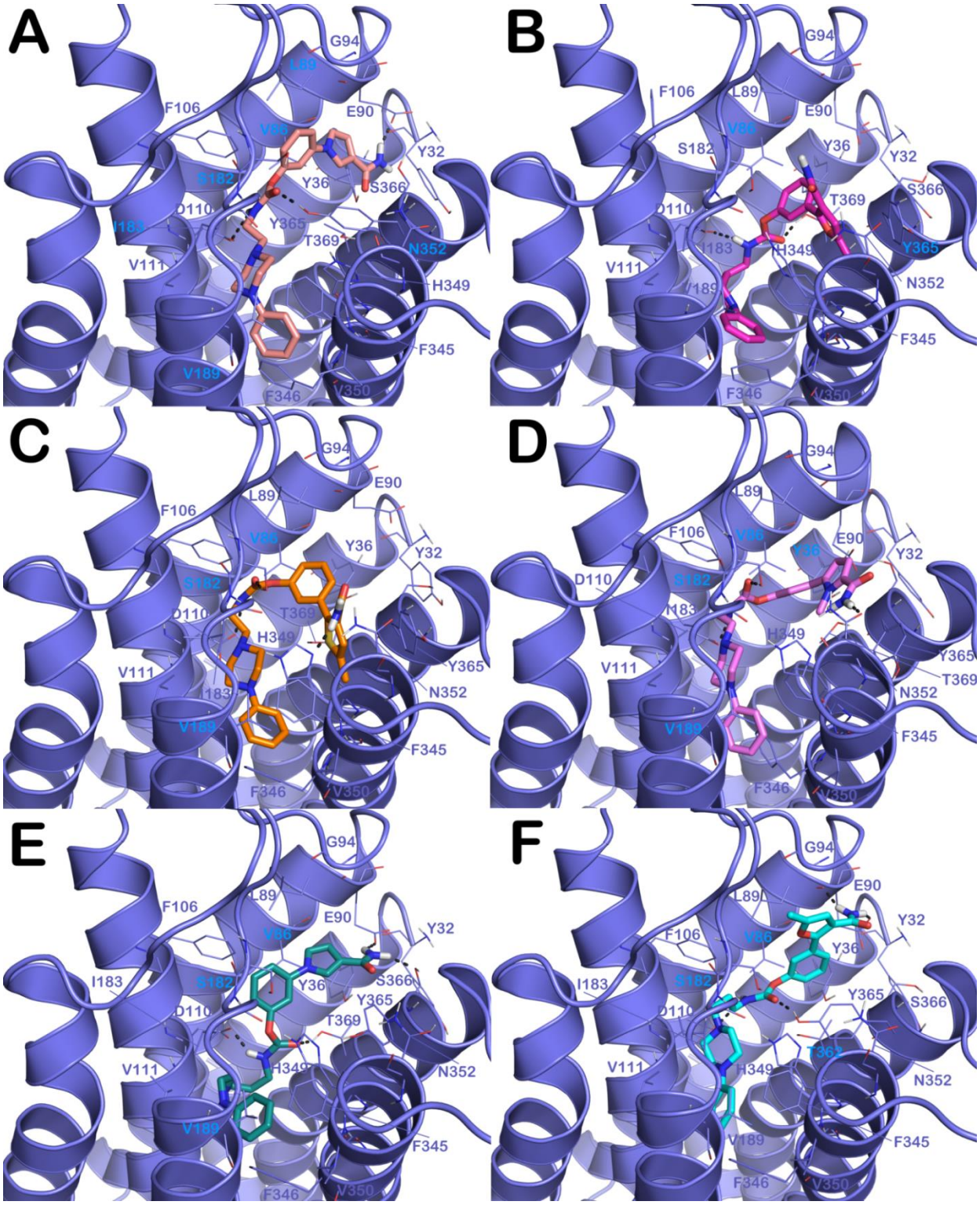

Figure 4. Binding modes of **5a** (light pink sticks, panel A), **5c** (magenta sticks, panel B), **5d** (orange sticks in panel C), **5h** (light magenta sticks, panel D), **5i** (dark green sticks, panel E) and **5j** (cyan sticks, panel F) into D_3 receptor binding site (purple cartoon, PDB ID: 3PBL). The residues forming the binding site are represented as lines. The non-polar hydrogens were removed for

clarity. The pictures were generated by means of PyMOL (The PyMOL Molecular Graphics System, v1.8.4.0, Schrödinger LLC, New York, 2015).

2.3 Drug-likeliness, selectivity and toxicity profile of selected analogues

In order to assess the drug-like profile of the developed compounds we evaluated, for selected analogues, some key features either *in silico* or by experimental methods. While physicochemical properties were computationally determined for all the new compounds **5a-j** (Table S1 of the Supplementary Material), some key features were experimentally determined for selected analogues such as: i) selectivity profile towards proteins of the ECS (Figure 5); ii) solubility and chemical stability (by HPLC methods, Table 2), iii) cytotoxicity and mutagenicity profile (Table 3 and Figure 6). We also performed preliminary metabolic stability studies (Figure 7 and Table S2_ and S3).

2.3.1. Selectivity profile (CB_1R, CB_2R, MAGL)

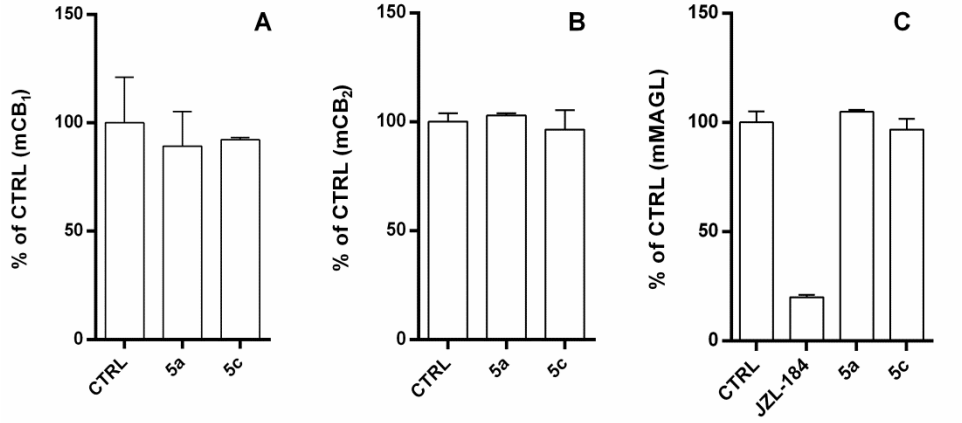

Figure 5. Selectivity of **5a** and **5c** towards *m*CB_1R (Panel A), *m*CB_2R (Panel B), and *m*MAGL (Panel C), data for JZL-184 a potent MAGL inhibitor is reported for comparison.

The selectivity profile was experimentally measured for compounds **5a** and **5c** towards the mouse cannabinoid receptors and the hydrolytic ECS enzyme MAGL. The *m*CB_1R and *m*CB_2R share, as

based on sequence alignments (source: uniprot), a high level of identity with the human isoforms 97.0% for the CB_1R and 79.7 for the CB_2R. As clearly depicted in Figure 5, these studies allowed us to exclude, for **5a** and **5c**, any interaction with either the cannabinoid receptors or the MAGL enzyme.

2.3.2. In silico prediction and experimental evaluation of selected drug-like properties

Some molecular properties were calculated by means of QikProp and our proprietary 3D-QSAR model (3D-chERGi) to assess the affinity for *h*ERG K^+ channel.

The predicted molecular properties evidenced improved aqueous solubility (cLogS) and cLogP, compared to reference compound **3a**. No violations of Lipinski's rules were found, and the human oral adsorption was considered acceptable.

With these data in hands we decided to undertake *in vitro* assessments of selected drug-like properties. The solubility (at pH = 3 and pH = 7.4, Table 2) and the chemical stability (at pH = 3, Table 2) of compound **5c** were measured by means of HPLC methods.[38] As predicted, the presence of the basic phenylpiperazine system improved the solubility profile of **5c** over that of **3a**. The same was also true for compound **5a** (**5a** solubility at pH = 3 was 574 µM). Gratifyingly, our analyses also revealed that both **3a** and **5c**, bearing a carbamoyl functionality, exhibited a favorable chemical stability profile at acidic pH. In particular, the chemical stability was almost quantitative for compound **5c** with 99.9% remaining unaltered after 24 h at pH = 3.

Table 2. Solubility and chemical stability of compounds **5c** and **3a**

Cmpd	**Solubility (µM)** after 12 h	**Chemical Stability (%)** after 24 h

	pH = 3	pH = 7.4	pH = 3
3a	465	n.c.[a]	92.1
5c	991	2	99.9

n.d.[a] = not calculable, below the quantitation limit.

As a preliminary safety evaluation, we assessed *in silico* the potential interaction of the newly developed compounds with the *h*ERG potassium channels using the recently developed 3D-QSAR model, namely 3D-chERGi. It is well established that sustained interaction with this membrane protein is responsible for a fatal cardiac arrhythmia (torsade-de-pointes) and this kind of evaluation is currently a key point in the early drug discovery trajectory. In general, when tested *in silico*, the new compounds (Table S1) were predicted by the 3D-chERGi to possess from moderate to low affinity for the *h*ERG channel. Of note, the highest predicted affinities were found for compounds **5d**, **5f** and **5i** (Table S1).

These results prompted us to experimentally determine the IC_{50} values for *h*ERG from patch clamp studies (Table 1 last column). As a whole, these studies were in good agreement with the predicted *in silico* data and revealed that amongst the new compounds, although in general more active than the parent analogues **3a**,**b**, the compounds **5a**, **5h** and **5i** were the best performing of the new series (exhibiting IC_{50} values of 5.3, 6.4 and 3.5 µM respectively, Table 1). On the other hand, **5c** and **5d**, in line with our *in silico* predictions, exhibited submicromolar IC_{50} values.

*Cytotoxicity and mutagenicity profile evaluation for **3a**, **5a**, and **5c***

Besides the physico-chemical parameters of the compounds, we experimentally determined addition al features that might contribute to designate the most promising compounds **5a** and **5c** as potential hits of the series. To this aim we determined their potential cytotoxicity profile after incubation with mouse embryonic fibroblasts (NIH3T3 cell line), and with human glioblastoma astrocytoma cells (U373MG cell line). The viabilities of these cells, after incubation with **5a** and **5c**, are reported in Ta

ble 3 and are expressed as IC_{50} (μM). The values are compared with those obtained for the FAAH i nhibitor **3a**.

Table 3. Viability of mouse fibroblasts NIH3T3 and human glioblastoma astrocytoma cells U373-MG after incubation with **5a**, **5c** and **3a** (as IC_{50} μM).

	NIH3T3[a]	**U373MG**[a]
Cmpds	**IC_{50} (μM)**	**IC_{50} (μM)**
3a	75	50
5a	5	NT
5c	68	23

[a]Cell viability was measured by the Neutral Red Uptake (NRU) test and data normalized as % control; data are expressed as mean ± SD of three experiment repeated in six replicates; values are statistically different *vs* control, $p \leq 0.05$.

We observed that **5a** and **5c** showed toxicities only in the μM range. In particular, **5a** was found more toxic than **3a** on the NIH3T3 cell line, while **5c** exhibited a two-digit μM toxicity on both cell lines, being as low as that **3a** for NIH3T3 cells. All these tests were performed with concentrations of the tested compounds ranging from 4 to 100 μM.

As a further profiling, we ascertained for **5a** the lack of mutagenic effect in the *Salmonella typhimurium strains* TA98 and TA100. The Ames test is designed to identify potential risks of mutagenicity at the early stages of drug development. The assay can be performed in presence or not of the S9 fraction of rat liver. This latter condition is a more in-depth investigation for assessing the potential mutagenicity risks derived from the compound's metabolites. After applying both experimental conditions, we did not observe any mutagenic effect for compound **5a** at all the concentrations tested (5-230 μM) (Figure 6A-D).

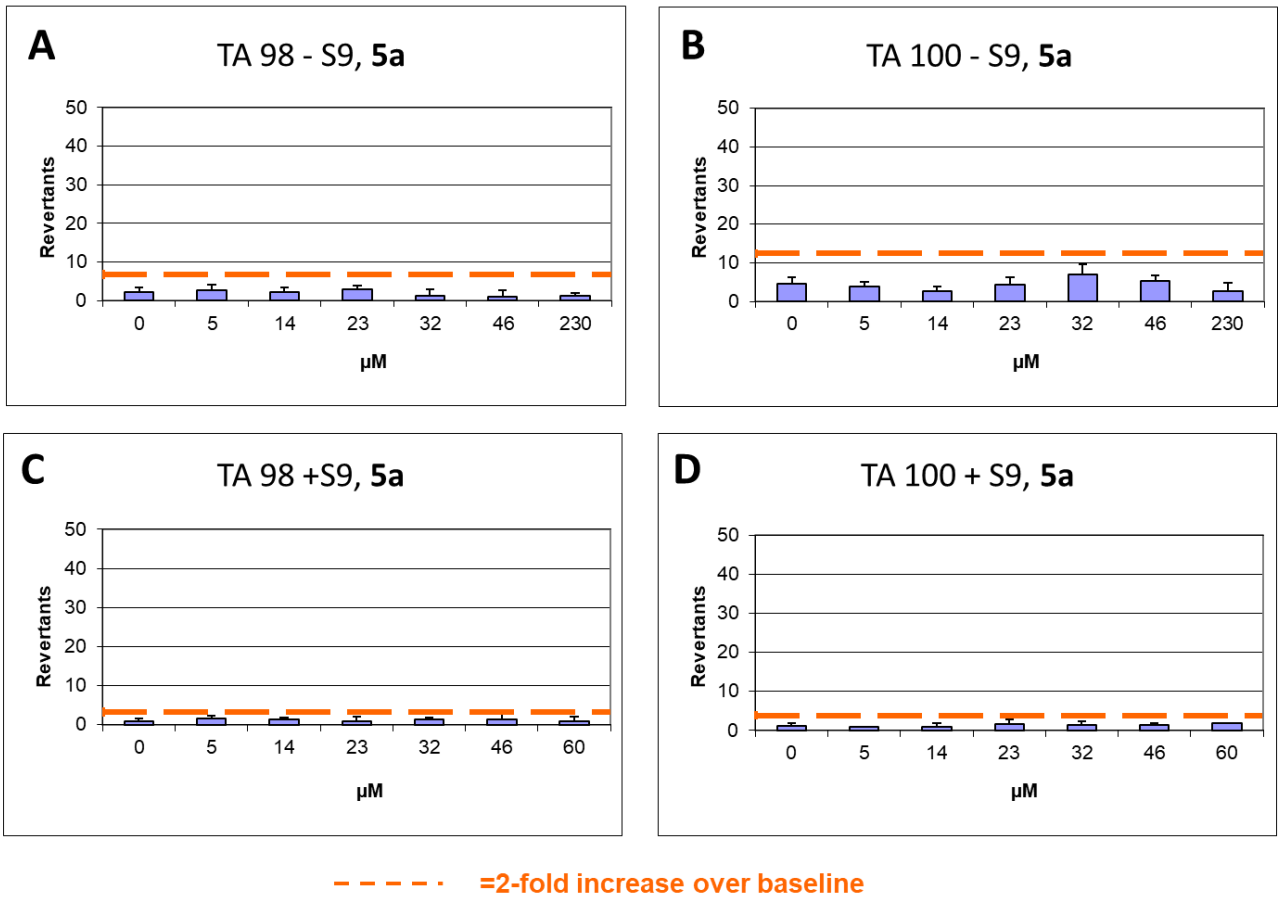

Figure 6. Ames test performed on *S. typhimurium* TA98 and TA100 strains for compounds **5a**.

2.4. Preliminary metabolic studies.

*In silico and in vitro evaluation of potential site of metabolism of **3a** and **5c***

In order to further characterize the most promising analogue **5c**, we computationally investigated the potential sites of metabolism and **5c** in comparison with those of **3a**. It is well established that cytochrome P450 enzymes are crucial in the metabolism of drugs. For this purpose, we employed P450 site of metabolism (P450 SOM) application implemented in Schrödinger suite 2018. As previously demonstrated by us,[39, 40] this application is very useful in predicting potential soft spots when aiming at understanding the liable sites of the molecules.

We predicted metabolism mediated by isoforms CYP3A4, CYP2C9, and CYP2D6 of compounds **3a** and **5c**. The prediction for isoforms CYP2C9 and CYP2D6 combined IFD (for determining the compounds' accessibility to the CYP reactive centre) with a rule-based approach to intrinsic

reactivity. In the case of CYP3A4, which has a highly flexible binding site, only intrinsic reactivity was used to predict soft spots. Moreover, the MetaSite 6.0.1 prediction of the metabolites in liver was also performed for the same compounds.

Based on the calculations (the outputs are reported in Table S2), we can speculate that the metabolism of **3a** and **5c** is mainly mediated by the isoforms CYP3A4 and CYP2C9. For both compounds the *para* positions on the terminal phenyl rings could represent the main soft spots, and compound **5c** appeared to be more susceptible to the CYP-mediated metabolism, with respect to compound **3a**, since for **5c** extra potential soft spots were found on the piperazine system. The MetaSite 6.0.1 prediction of the metabolites in liver overlapped the previously described results and it also evidenced that for compound **3a** the site of metabolism was preferentially located on the *C* atom in α-position with respect to the terminal benzene group and in the *C* atom close to the carbamoyl *N* in the aliphatic chain. For compound **5c** the most probable metabolites could derive from hydroxylation on the terminal aromatic moieties and/or in the furan system.

To this *in silico* approach we combined *in vitro* studies assessing the metabolic stability of **3a** and **5c** in human and rat liver microsomal preparations (HLM and RLM). The plot of non-metabolized compound [natural logarithm of % of compound recovery (100% at time 0 min)] as a function of incubation time showed monoexponential decay relationship for both substrates (Figure 7). The apparent decay constants (k) half-life time (t½) and intrinsic clearance (CLint) are reported in Table 4. Compound **5c** presented very similar kinetic parameters in both preparations. On the contrary, compound **3a** was slowly metabolized by RLM. In fact, the resulted t½ were 50.26 min in RLM and 27.77 in HLM, respectively. However, the incubation of both compounds in HLM gave rise to a comparable behavior and the intrinsic clearances were quite similar (41.6 and 47.4 μL/min/mg protein for **3a** and **5c**, respectively).

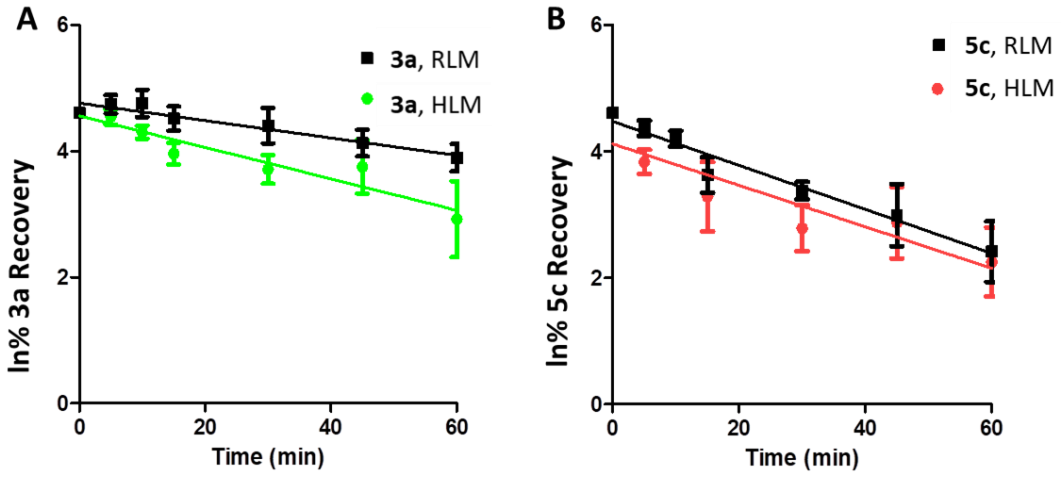

Figure 7. CYP-dependent metabolic depletion of 5 μM **3a** (panel A) and **5c** (panel B) in human (HLM) and rat liver (RLM) microsomal preparations. Results are presented graphically as percentage of compound recovery (100% at time 0 min) as a function of incubation time. Data are presented as mean ± SEM, of three different experiments.

Table 4. Kinetic parameters and metabolic stability of compounds **3a** and **5c**.

Cmpd	**RLM**			**HLM**		
	k (min^{-1})	CL_{int} (μL/min/mg prot.)	$t_{1/2}$ (min)	k (min^{-1})	CL_{int} (μL/min/mg prot.)	$t_{1/2}$ (min)
3a	0.01379	23.45	50.26	0.02496	41.60	27.77
5c	0.03482	59.22	19.91	0.02842	47.36	24.39

These results clearly indicate that the two compounds should be considered moderate substrate of CYP450 system as resulted from their intrinsic clearance value.[41] Interestingly the introduction of a phenylpiperazine moiety in the molecule, needed for modulating the pharmacological profile and improving the water solubility, did not modify the metabolic stability in human liver. The results suggest that both compounds could possess favorable pharmacokinetic properties, at least regarding their interaction with phase I enzyme system.

A preliminary qualitative HPLC/ESI-MS analysis for identifying potential metabolites was performed on the medium obtained after incubation of the compounds **3a** and **5c** (with incubation

time of 0 and 30 min at 50 μM). The data reported in Table S3, show that some amount of the tested compounds remains after 30 min of incubation. Few metabolites were identified that flanked the presence of the parent compounds and namely: i) the phenol derivative, originated following *N*-dealkylation and decarboxylation process, ii) a mono-hydroxylated metabolite, and iii) a phenylpiperazine chain was evident for compound **5c**. For both analyzed compounds the mono-hydroxylated analogue was present only in the medium that was incubated 30 min with the HLM.

*2.5. Evaluation of anti-inflammatory potential for compound **3a** and **5c**.*

Though some treatments are available for nicotine dependence, there are high rates of relapse. Nicotine dependence has been frequently associated to stress[42] and several evidences show that the rewarding properties of nicotine are increased under stress conditions and that the stress factors can alter neurotransmitter systems including dopaminergic and serotoninergic systems. Notably, the mechanisms underlying nicotine dependence and major depressive disorders appear to involve common alterations in neurotransmitter pathways.[42] A great body of evidences point out that nicotine induces oxidative stress (OS) and the production of reactive oxygen species not only in the periphery but also in CNS structures involved in emotional and cognitive processes, such as the prefrontal cortex and hippocampus.[43] In humans, OS markers have been associated with both depression and smoking and have been linked to nicotine dependence.[43] The nicotine pro-oxidative effects have also been demonstrated in animals *in vivo* (in liver, kidneys, heart, and in the CNS),[44] where after acute and subchronic nicotine treatment it induced OS and inflammation within brain structures responsible for emotional and cognitive processes.[45] On these bases it was also envisaged that anti-inflammatory drugs could serve as efficient and novel treatment for nicotine dependence.

Cigarette smoking induces an excess of pro-inflammatory cytokines, pro-inflammatory gene transcription, and OS.[46] Exposure to OS from cigarette smoke also impacts the NF-κB pathway,[47] and activates inflammatory immune response contributing to additional endogenous oxidants formation.[48] The above considerations point out that OS and inflammation are relevant

issues in most human diseases and are also pivotal in drug and nicotine addictions.[46] Therefore, we interrogated the ability of one of the most promising compounds of the series (**5c**) to modulate the inflammation process and we compared its effect with that induced by our reference compound **3a**. Prior to the evaluation of the anti-inflammatory potential of compounds **3a** and **5c** in the IMR 32 cells, we performed a cytotoxicity assay to exclude any toxic effect on the same cell line. Accordingly, IMR 32 cells were treated with compounds **3a** and **5c** in a range of concentrations between 0.1 and 50 µM. As depicted in Figure 8, both compounds did not affect significantly the release of LDH from IMR 32 cells at any of the tested concentrations, thus allowing us to exclude any cytotoxic effect for the tested compounds. Based on these results we performed the next experiments aiming at evaluating the potential anti-inflammatory properties at the doses of 0.5 µM and 1 µM.

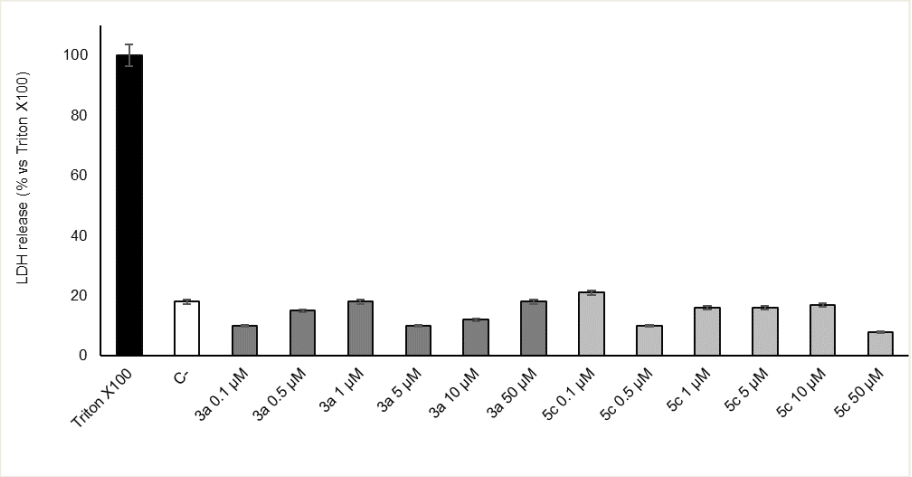

Figure 8. Cytotoxicity determined as LDH release in IMR 32 cells treated for 24 h with compounds **3a** and **5c** at different concentrations (0.1, 0.5, 1, 5, 10 and 50 µM). Values represent average +/- SD of samples performed at least in triplicate. Data are expressed as percentage of LDH release as compared to the maximum release of LDH from Triton X-100- treated cells (100%).

To test the anti-inflammatory properties of compounds **3a** and **5c**, IMR 32 cells were first pre-treated with the compounds of interest at the doses of 0.5 µM and 1 µM for 24 h. After the pre-treatment, IMR 32 cells were challenged with 100 µg/mL LPS for 30 min and the activation of NF-

κB was evaluated by NF-κB-DNA binding. As shown in Figure 9, LPS increased the binding activity of nuclear extracts to the NF-κB-DNA consensus sequence. Pre-treatment with the compounds **3a** and **5c** for 24 h significantly inhibited LPS-inducible NF-κB p65 DNA binding in IMR 32 cells as also confirmed by immunoblotting analysis (data not shown). These experiments allowed us to ascertain a dose dependent inhibition of NF-κB p65 DNA binding for both compounds, which showed a similar anti-inflammatory effect.

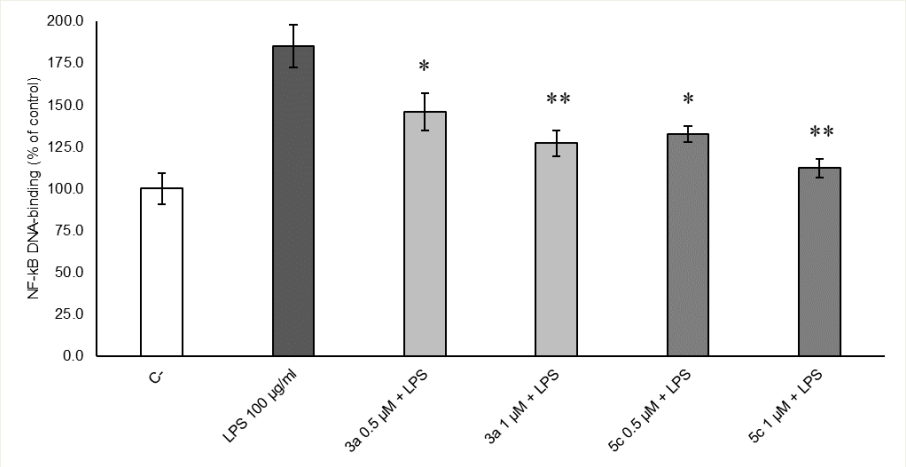

Figure 9. NF-κB-DNA-Binding levels in nuclear extracts from IMR 32 cells pre-treated with compounds **3a** and **5c** for 24 h and challenged with 100 µg/mL LPS for 30 min. Data are presented as mean ± SEM of 3 independent experiments. * $p < 0.05$ vs LPS treatment; **$p < 0.01$ vs LPS treatment.

3. Conclusions

We have herein reported the identification and SAR analysis of a new class of phenyl heterocyclic compounds bearing an arylpiperazine moiety behaving as multipotent tools (FAAH inhibitors and D_2/D_3 receptor ligands, compounds **5a-j**). Biological characterization on the targets of interest, selectivity profile towards proteins of the ECS (CB_1R, CB_2R and MAGL), *h*ERG channel liability evaluation, together with the *in silico* assessment of the drug-likeliness profile allowed the selection of the best performing analogues. The selected analogues, **5a** and **5c**, in comparison with our lead FAAH inhibitor **3a**, were further assessed in vitro in living cells. These studies exclude toxic effects

on mouse fibroblasts NIH3T3 and human glioblastoma astrocytoma cells U373-MG 3T3. Gratifyingly, as based on the results of the cellular studies in the conditions of the Ames tests, we could assume the lack of mutagenicity as well. Preliminary metabolic studies were performed on compounds **3a** and **5c** after incubation with RLM and HLM. In line with the *in silico* predicted metabolic liabilities, the compounds behaved as moderate substrates of CYP450 system (as indicated by their intrinsic CLint values). Notably, the introduction of a phenylpiperazine moiety in the molecule, needed for modulating the pharmacological profile and improving the water solubility, did not negatively affect the metabolic stability in human liver, thus suggesting that **5c** could possess a favorable pharmacokinetic profile, at least regarding their interaction with phase I enzyme system. To finally complement the profile of the compounds **3a** and **5c** we assessed their anti-inflammatory properties on IMR 32 cells, where we could demonstrate their ability to reduce the LPS-induced activation of the redox-sensitive transcription factor NF-κB.

4. Experimental Part

4.1. Chemistry.

4.1.1. General procedures.

Unless otherwise specified, materials were purchased from commercial suppliers and used without further purification. Reaction progress was monitored by TLC using silica gel 60 F254 (0.040–0.063 mm) with detection by UV. Silica gel 60 (0.040–0.063 mm) was used for column chromatography. ^{1}H NMR and ^{13}C NMR spectra were recorded on a Varian 300 MHz spectrometer or a Bruker 400 MHz spectrometer by using the residual signal of the deuterated solvent as internal standard. Splitting patterns are described as singlet (s), doublet (d), triplet (t), quartet (q) and broad (br); the values of chemical shifts (δ) are given in ppm and coupling constants (*J*) in Hertz (Hz). HPLC were performed with a Shimadzu Prominence apparatus equipped with a scanning absorbance UV-VIS detector (Diode Array SPD-M20A) also equipped with a thermostatic chamber and with Agilent 1100 Series equipped with UV-VIS detector. ESI-MS spectra were performed by

an Agilent 1100 Series LC/MSD spectrometer. HRESIMS were carried out by a Thermo Finningan LCQ Deca XP Max ion-trap mass spectrometer equipped with Xcalibur software, operated in positive ion mode. The yields are referred to purified products and are not optimized. All moisture-sensitive reactions were performed under argon atmosphere using oven-dried glassware and anhydrous solvents. Final compounds were analyzed by combustion analysis (CHN) to confirm purity >95%.

*4.1.2. 2-(4-Phenylpiperazine-1-yl)ethanamine (**7a**).*

2-(4-Phenylpiperazine-1-yl)acetonitrile. To a solution of phenylpiperazine **6** (1.27 mL, 8.33 mmol) in EtOH (40.0 mL), Na_2CO_3 (1324.0 mg, 12.49 mmol) and bromoacetonitrile (580.0 µL, 8.33 mmol) were sequentially added. The reaction mixture was stirred under N_2 atmosphere for 2 h at 25 °C. The inorganic salt precipitate was filtered and washed with EtOH. The filtrate was concentrated, and the residue taken up with H_2O. The aqueous phase was extracted with EtOAc (3 x 10 mL). The combined organic layers were washed with a saturated solution of NaCl, dried over anhydrous sodium sulphate, filtered and concentrated. The crude was purified by column chromatography on silica gel (petroleum ether/EtOAc 4:1). 2-(4-Phenylpiperazine-1-yl)-acetonitrile was obtained as an amorphous orange solid (70% yield). ^{1}H NMR (400 MHz, $CDCl_3$) δ 7.30-7.24 (m, 2H, ArH), 6.95-6.86 (m, 3H, ArH), 3.58 (s, 2H, CN-CH_2), 3.25 (t, *J* = 4.8 Hz, 4H, ArN-$(CH_2)_2$ piperazine), 2.77 (t, *J* = 5.1 Hz, 4H, N-$(CH_2)_2$ piperazine). ESI-MS *m/z*: 189 $[M+Na]^+$. 2-(4-Phenylpiperazine-1-yl)-acetonitrile (3.28 g, 16.33 mmol) was dissolved in dry THF (65.3 mL) and the solution thus obtained was added dropwise to a suspension of $LiAlH_4$ (1.24 g, 32.65 mmol) in dry THF (49.0 mL) at 0 °C. The mixture was then warmed to 25 °C and the reaction was stirred under N_2 atmosphere for 2 h. The reaction was quenched by adding water dropwise at 0 °C. Subsequently, 15% NaOH was added until pH = 9. The resulting precipitate was filtered by means of a celite pad and the filtrate washed with EtOAc and then concentrated. The residue was purified by means of column chromatography on silica gel (DCM/MeOH, 7:3) to afford the title compound **7a** as a white

amorphous solid (50% yield). ^{1}H NMR (400 MHz, $CDCl_3$) δ 7.26 (t, *J* = 6.9 Hz, 2H, ArH), 6.92 (d, *J* = 8.1 Hz, 2H, ArH), 6.85 (t, *J* = 7.2 Hz, 1H, ArH), 3.21-3.18 (m, 4H, ArN-$(CH_2)_2$ piperazine), 2.82 (t, *J* = 6.0 Hz, 2H, CH_2), 2.63-2.60 (m, 4H, N-$(CH_2)_2$ piperazine), 2.48 (t, *J* = 5.7 Hz, 2H, CH_2). ESI-MS *m/z*: 206 $[M+H]^+$. *4.1.3. 3-(4-Phenylpiperazin-1-yl)propan-1-amine (**7b**).*

Compound **7b** was prepared starting from phenylpiperazine and bromopropionitrile following the same procedure described for **7a**. ^{1}H NMR (400 MHz, $CDCl_3$) δ 7.27-7.24 (m, 2H, ArH), 6.92-6.90 (d, *J* = 8.4 Hz, 2H, ArH), 6.86 (t, *J* = 7.2 Hz, 1H, ArH), 3.19 (t, *J* = 5.2 Hz, 4H, ArN-$(CH_2)_2$ piperazine), 2.96 (t, *J* = 6.0 Hz 4H, N-$(CH_2)_2$ piperazine), 2.65 (t, *J* = 5.2 Hz, 2H, CH_2-NH_2), 2.56 (t, *J* = 6.4 Hz, 2H, CH_2-N), 1.83-1.76 (q, *J* = 6.4 Hz, 2H, CH_2 chain).

*4.1.4. N-(2-(4-Phenylpiperazin-1-yl)ethyl)-1H-imidazole-1-carboxamide (**8**).*

Amine **7a** (100.0 mg, 0.49 mmol) was dissolved in H_2O (35.0 mL) at 25 °C. The solution was cooled to 0 °C and CDI (158.0 mg, 0.98 mmol) was added. The resulting mixture was kept under magnetic stirring at 0 °C, until a white precipitate was observed. After filtration under vacuum, the precipitate was washed with cold water, affording pure compound as an amorphous white solid (90% yield). ^{1}H NMR (300 MHz, $CDCl_3$) δ 8.11 (s, 1H, imidazol-CH), 7.32-7.25 (m, 3H, ArH), 7.09 (s, 1H, imidazol-CH), 6.94.6.86 (m, 3H, ArH, imidazole-CH), 6.55 (br s, 1H, NHCO), 3.59-3.53 (m, 2H, CH_2-NH), 3.23-3.20 (m, 4H, ArN-$(CH_2)_2$ piperazine), 2.70-2.67 (m, 6H, N-$(CH_2)_2$, CH_2 piperazine). ESI-MS *m/z*: 322 $[M+Na]^+$. *4.1.5. 3-(3-Carbamoyl-1H-pyrrol-1-yl)phenyl (2-(4-phenylpiperazin-1-yl)ethyl)carbamate (**5a**).*

To a solution of **9** (50.0 mg, 0.25 mmol) and DMAP (121.0 mg, 0.99 mmol) in dry THF (18.0 mL) at 0 °C, phosgene (20% in toluene, 243.0 μL, 0.46 mmol) was added. After warming up to 25 °C, the reaction was stirred for 30 min. under N_2 atmosphere. Amine **7a** (101.5 mg, 0.49 mmol) was then added and the mixture was refluxed for further 12 h. Evaporation and silica gel column chromatography (100% EtOAc to EtOAc/MeOH 95: 5) afforded the title compound as an amorphous white solid (20% yield). ^{1}H NMR (300 MHz, $CDCl_3$) δ 7.64 (s, 1H, pyrrol-CH), 7.42 (t,

J = 8.7 Hz, 1H, ArH), 7.30-7.23 (m, 4H, ArH, pyrrol-CH), 7.11 (dd, *J* = 2.1 Hz, 8.7 Hz, 1H, ArH), 7.03-7.02 (m, 1H, ArH), 6.94 (d, *J* = 8.4 Hz, 2H, ArH), 6.87 (t, *J* = 7.2 Hz, 1H, ArH), 6.54-6-52 (m, 1H, pyrrol-CH) 5.71-5.55 (br s, 3H, $CONH_2$, OCONH), 3.46-3.41 (m, 2H, CH_2-NH), 3.25-3.22 (m, 4H, ArN-$(CH_2)_2$ piperazine), 2.69-2.61 (m, 6H, N-$(CH_2)_2$ piperazine, CH_2). ^{13}C NMR (75 MHz, $CDCl_3$) δ 166.7, 154.4, 152.2, 151.3, 140.8, 130.6, 129.4, 122.9, 120.9, 120.2 (2), 117.7, 116.4, 114.8, 109.8, 57.0, 53.1, 49.2, 37.8. ESI-MS *m/z:* 434 $[M+H]^+$. HRMS-ESI *m/z*: $[M+H]^+$ calcd for $C_{24}H_{28}N_5O_3$ 433,2114; found 434,2175. Anal. ($C_{24}H_{27}N_5O_3$) C, H, N.

*4.1.6. 3-(3-Carbamoyl-1H-pyrrol-1-yl)phenyl (3-(4-phenylpiperazin-1-yl)propyl)carbamate (**5i**).*

Compound **5i** was prepared following the procedure employed for the preparation of compound **5a**, starting from phenol **9** and amine **7b**. ^{1}H NMR (300 MHz, $CDCl_3$) δ7.62 (pyrrol-CH s, 1H), 7.43 (t, *J* = 8.7 Hz, 1H, ArH), 7.18-7.28 (m, 4H, ArH, pyrrol-CH), 6.98-7.09 (m, 2H, ArH), 6.92 (d, *J* = 8.4 Hz, 2H, ArH), 6.88 (m, 1H), 6.62 (br s, 1H, OCONH), 6.54-6-52 (m, 1H, pyrrol-CH)5.61 (br s, 2H, $CONH_2$), 3.43-3.38 (m, 2H, CH_2-NH), 3.23-3.19 (m, 4H, ArN-$(CH_2)_2$ piperazine), 2.65-2.57 (m, 6H, N-$(CH_2)_2$ piperazine, CH_2-N), 1.81 (m, 2H, CH_2 chain). ^{13}C NMR (75 MHz, $CDCl_3$) δ 166.5, 154.3, 152.3, 151.3, 140.8, 130.5, 129.4, 122.9, 120.9, 120.2, 120.1, 117.6, 116.3, 114.9, 109.8, 57.6, 53.5, 49.4, 41.6, 25.5. Anal. ($C_{25}H_{29}N_5O_3$) C, H, N.

*4.1.7. 1-(3-Aminophenyl)-1H-pyrrole-3-carboxamide (**11**).*

1-(3-Nitrophenyl)-1H-pyrrole-3-carbonitrile was prepared starting from **10** and 3-nitroaniline according to a described procedure[24] (92% yield, brown oil). ^{1}H NMR (300 MHz, $CDCl_3$) δ 7.41 (s, 1H, pyrrol-CH), 7.18 (t, *J* = 8.1 Hz, 1H, ArH), 6.96 (t, *J* = 2.5 Hz, 1H, ArH), 6.72 – 6.59 (m, 3H, ArH, pyrrol-CH), 6.54 – 6.50 (m, 1H, pyrrol-CH). ESI-MS *m/z*: 236 $[M+Na]^+$.

For the synthesis of *1-(3-aminophenyl)-1H-pyrrole-3-carbonitrile* the previously obtained *1-(3-nitrophenyl)-1H-pyrrole-3-carbonitrile* (153.0 mg, 0.72 mmol) was dissolved in EtOH (10.0 mL) and tin(II) chloride dihydrate (810.0 mg, 3.59 mmol) was added. The reaction mixture was refluxed for 2 h. After cooling to 25 °C, the mixture was poured in an ice bath, and 10% aqueous $NaHCO_3$

was added up to pH = 8. After filtration through a Celite pad and EtOH evaporation under vacuum, the aqueous layer was extracted with DCM (3 x 10 mL). The combined organic layers were washed with a saturated solution of NaCl, dried over anhydrous sodium sulphate, filtered and concentrated. The obtained *1-(3-aminophenyl)-1H-pyrrole-3-carbonitrile* was used in the next step without any further purification (95% yield, yellow oil). ^{1}H NMR (300 MHz, $CDCl_3$) δ 7.41 (s, 1H, pyrrol-CH), 7.18 (t, *J* = 8.1 Hz, 1H, ArH), 6.96 (d, *J* = 2.5 Hz, 1H, ArH), 6.70 – 6.60 (m, 3H, ArH, pyrrol-CH), 6.54 – 6.49 (m, 1H, pyrrol-CH), 3.96 (br s, 2H, Ar-NH_2). ESI-MS *m/z*: 206 [*M*+Na]$^+$.

To a solution of *1-(3-aminophenyl)-1H-pyrrole-3-carbonitrile* (65.0 mg, 0.35 mmol) in EtOH (22.0 mL), 6M NaOH (867 µL) and 30% H_2O_2 (867 µL) were added. The reaction mixture was refluxed for 3 h. After cooling to 25 °C, a saturated solution of $Na_2S_2O_3$ (2.0 mL) was added and the solvent was evaporated under reduced pressure. The residue was taken up with H_2O and extracted with EtOAc (3 x 5 mL). The combined organic layers were washed with a saturated solution of NaCl, dried over anhydrous sodium sulphate, filtered and concentrated. The crude *1-(3-aminophenyl)-1H-pyrrole-3-carboxamide* **11** was used in the next step without any further purification as yellow solid (90% yield). ^{1}H NMR (300 MHz, $CDCl_3$) δ 7.69 – 7.53 (m, 1H, pyrrol-CH), 7.20 (t, *J* = 8.0 Hz, 1H, ArH), 7.03 – 6.94 (m, 1H, pyrrol-CH), 6.82 – 6.73 (m, 1H, ArH), 6.68 (d, *J* = 2.1 Hz, 1H, ArH), 6.65 – 6.58 (m, 1H, ArH), 6.56 – 6.47 (m, 1H, pyrrol-CH), 5.53 (br s, 2H, $CONH_2$), 3.82 (br s, 2H, $ArNH_2$). ESI-MS *m/z*: 224 [*M*+Na]$^+$.

*4.1.8. 1-(3-(3-(2-(4-Phenylpiperazin-1-yl)ethyl)ureido)phenyl)-1H-pyrrole-3-carboxamide (**5b**).*

Compound **11** (25.0 mg, 0.12 mmol) was dissolved in dry THF (10.0 mL). Then TEA (67 µL, 0.50 mmol) and, after cooling to 0 °C, phosgene (20% in toluene, 130 µL, 0.25 mmol) were added. The reaction mixture was stirred at 25 °C for 1 h. Amine **7a** was then added and the reaction mixture was stirred for further 12 h at the same temperature. Evaporation followed by silica gel column chromatography (DCM/MeOH 9:1) afforded the pure title compound as colourless oil (20% yield). ^{1}H NMR (400 MHz, $CDCl_3$) δ 7.81 (br s, 1H, ArNHCO), 7.60 (d, *J* = 29.1 Hz, 1H, pyrrol-CH),

7.39 – 7.20 (m, 5H, ArH, pyrrol-CH), 7.07 – 6.80 (m, 5H, ArH), 6.48 (s, 1H, pyrrol-CH), 6.16 (br s, 1H, NHCO), 5.87 (br s, 2H, $CONH_2$), 3.49 – 3.47 (m, 2H, CH_2-NH), 3.24 (br s, 4H, ArN-$(CH_2)_2$ piperazine), 2.81-2.65 (m, 6H, N-$(CH_2)_2$ piperazine, CH_2-N). ESI-MS *m/z:* 433 $[M+H]^+$. Anal. ($C_{24}H_{28}N_6O_2$) C, H, N.

*4.1.9. 3-(3-Carbamoyl-5-methylfuran-2-yl)phenyl (2-(4-phenylpiperazin-1-yl)ethyl)carbamate (**5c**).*

Compound **12a** (50.0 mg, 0.23 mmol) was dissolved in dry THF (18.6 mL) and DMAP (112.6 mg, 0.92 mmol) was added. After cooling to 0 °C, phosgene (20% solution in toluene, 243 μL, 0.46 mmol) was added. The reaction mixture was allowed to warm to 25 °C and then stirred for 30 min under N_2 atmosphere. Amine **7a** (94.5 mg, 0.46 mmol) was then added and the reaction mixture was refluxed for 12 h. The solvent was removed and the crude was purified by column chromatography on silica gel (form 100% EtOAc to EtOAc/MeOH 95:5) to obtain **5c** as an amorphous white solid (30% yield). ^{1}H NMR (300 MHz, $CDCl_3$) δ 7.67-7.62 (m, 2H, ArH), 7.41 (t, *J* = 8.1 Hz, 1 H, ArH), 7.30-7.23 (m, 2H, ArH), 7.14 (dd, *J* = 1.5, 8.1 Hz, 1H, ArH), 6.94 (d, *J* = 7.8 Hz, 2H, ArH), 6,86 (t, *J* = 7.2 Hz, 1H, ArH), 6.33 (s, 1H, furan-CH), 5.76-5.65 (br s, 2H, $CONH_2$), 5.49 (br s, 1H, OCONH), 3.45-3.41 (m, 2H, CH_2-NH), 3.24-3.21 (m, 4H, Ar-N$(CH_2)_2$ piperazine), 2.68-2.60 (m, 6H N-$(CH_2)_2$ piperazine, CH_2-N), 2.34 (s, 3H, CH_3). ^{13}C NMR (75 MHz, $CDCl_3$) δ 165.8, 154.6, 152.2, 151.5, 151.4 (2), 131.3, 129.8, 129.4, 124.7, 122.3, 121.3, 120.1, 118.1, 116.3, 108.4, 57.0, 53.2, 49.4, 37.9, 13.6. ESI-MS *m/z*: 471 $[M+Na]^+$. Anal. ($C_{25}H_{28}N_4O_4$) C, H, N.

*4.1.10. 3-(3-Carbamoyl-5-methylfuran-2-yl)phenyl (3-(4-phenylpiperazin-1-yl)propyl)carbamate (**5j**).*

The title compound was prepared according to the procedure described for **5c**, starting from phenol **12a** and amine **7b.** The product was obtained as an amorphous white solid. (32% yield). ^{1}H NMR (300 MHz, $CDCl_3$) δ 7.66-7.52 (m, 2H, ArH), 7.39 (t, *J* = 8.1 Hz, 1 H, ArH), 7.30-7.21 (m, 2H, ArH), 7.12 (m, 1H, ArH), 6.95 (d, *J* = 7.8 Hz, 2H, ArH), 6.88 (m, 1H, ArH), 6.50 (br s, 1H, OCONH), 6.32 (s, 1H, furan-CH), 5.76 (br s, 1H, $CONH_2$), 5.51 (br s, 1H, $CONH_2$), 3.45-3.38 (m,

2H, CH_2-NH), 3.26-3.18 (m, 4H, Ar-N(CH_2)$_2$ piperazine), 2.69-2.53 (m, 6H, N(CH_2)$_2$ piperazine), 2.32 (s, 3H, CH_3), 1.65 (m, 2H, CH_2 chain). ^{13}C NMR (75 MHz, $CDCl_3$) δ 165.8, 154.7, 152.1, 151.5, 151.4 (2), 131.2, 129.8, 129.4, 124.6, 122.4, 121.4, 120.1, 118.1, 116.3, 108.5, 57.5, 53.5, 49.4, 31.2, 25.6, 13.6. Anal. ($C_{26}H_{30}N_4O_4$) C, H, N.*4.1.11. 3-(3-Carbamoyl-5-methylthiophen-2-yl)phenyl (2-(4-phenylpiperazin-1-yl)ethyl)carbamate (**5d**).*

The title compound was prepared according to the procedure described for **5c**, starting from phenol **12b** and amine **7a**. The product was obtained as an amorphous white solid. (34% yield). ^{1}H NMR (300 MHz, CD_2Cl_2) δ 7.45-7.17 (m, 6H, ArH), 7.07 (s, 1H, tiophen-CH), 6.93 (d, *J* = 7.8 Hz, 2H, ArH), 6.84 (t, *J* = 7.2 Hz, 1H, ArH), 5.74 (br s, 1H, OCONH), 5.53 (br, 2H, $CONH_2$), 3.40-3.38 (m, 2H, CH_2-NH), 3.23-3.20 (m, 4H, Ar-N(CH_2)$_2$ piperazine), 2.67-2.60 (m, 6H, N-(CH_2)$_2$ piperazine), 2.48 (s, 3H, CH_3); ^{13}C NMR (75 MHz, CD_2Cl_2) 165.6, 154.4, 151.7, 151.5, 141.7, 139.7, 134.5, 132.7, 129.8, 129.2, 127.6, 126.4, 123.0, 122.1, 119.6, 116.1, 56.9, 53.13, 49.3 (2), 37.9, 29.9, 15.0. ESI-MS *m/z*: 465 [*M*+H]$^+$, 487 [*M*+Na]$^+$, 503 [*M*+K]$^+$. Anal. ($C_{25}H_{28}N_4O_3S$) C, H, N.

*4.1.12. Ethyl 2-(3-methoxyphenyl)-1,5-dimethyl-1H-pyrrole-3-carboxylate (**15**).*

In a sealed tube, to a mixture of **13** (300.0 mg, 1.08 mmol) and a catalytic amount of sulphamic acid, methylamine (33% solution in EtOH, 15.0 mL) was added at -6 °C. The reaction mixture was warmed to 25 °C and stirred for 2 h. EtOH was removed and the residue was taken up with EtOAc and washed with a saturated aqueous $NaHCO_3$ and then with 2N HCl. The combined organic phases were dried over anhydrous Na_2SO_4, filtered and concentrated. Silica gel column chromatography (*n*-hexane/EtOAc 9:1) afforded the title compound as an amorphous white solid (50% yield). ^{1}H NMR (300 MHz, $CDCl_3$) δ 7.33 (t, *J* = 7.2 Hz, 1H, ArH), 6.92 (t, *J* = 6.9 Hz, 2H, ArH), 6.87 (s, 1H, ArH), 6.41 (s, 1H, pyrrol-CH), 4.09 (q, *J* = 6.9 Hz, 2H, CH_2-ethyl), 3.81 (s, 3H, OCH_3), 3.31 (s, 3H, - N-CH_3), 2.26 (s, 3H, C-CH_3), 1.12 (t, *J* = 7.5 Hz, 3H, CH_3-ethyl). ESI-MS *m/z*: 274 [*M*+H]$^+$, 296 [*M*+Na]$^+$, 312 [*M*+K]$^+$, 569 [2*M*+Na]$^+$.

*4.1.13. 2-(3-Methoxyphenyl)-1,5-dimethyl-1H-pyrrole-3-carboxylic acid (**16**).*

Compound **15** (347.0 mg, 1.27 mmol) was dissolved in EtOH (30 mL) and water (10 mL) and NaOH (1.80 g, 44.49 mmol) was added. The reaction mixture was stirred for 8 h at 25 °C. After removal of the organic solvent, the aqueous residue was acidified to pH = 1 by means of 6M HCl. The aqueous layer was then extracted with EtOAc (3 x 10mL). The combined organic phases were washed with a saturated solution of NaCl, dried over sodium sulphate, filtered and concentrated to obtain acid **16** as a yellow solid. Title compound was obtained enough pure to be used in the next reaction without any further purification (99% yield). ^{1}H NMR (300 MHz, CD_3OD) δ 7.31 (t, *J* = 7.8 Hz, 1H, ArH), 6.96-6.92 (m, 1H, ArH), 6.87-6.85 (m, 2H, ArH), 6.33 (s, 1H, pyrrol-H), 3.80 (s, 3H, OCH_3), 3.30 (s, 3H,-N-CH_3), 2.25 (s, 3H, C-CH_3). ESI-MS *m/z*: 268 $[M+Na]^+$.

*4.1.14. 2-(3-Methoxyphenyl)-1,5-dimethyl-1H-pyrrole-3-carboxamide (**17**).*

To a solution of compound **16** (200.0 mg, 0.82 mmol) in dry DCM, TEA (227 μL, 1.63 mmol), EDC (234.73 mg, 1.22 mmol) HOBt (154.4 mg, 1.14 mmol) were sequentially added at 0 °C. The reaction mixture was stirred under N_2 atmosphere for 10 min at 0 °C. Then 2.81 mL of conc. NH_4OH was added and the mixture was stirred for 30 min at 0 °C and for 16 h at 25 °C. Evaporation followed by silica gel column chromatography (petroleum ether/EtOAc 2:3) afforded the title compound as a light yellow solid (73% yield). ^{1}H NMR (300 MHz, $CDCl_3$) δ 7.40-7.38 (m, 1H, ArH), 7.01-6.91 (m, 3H, ArH), 6.47-6.43 (m, 1H, ArH), 5.06 (br s, 2H, $CONH_2$), 3.83 (s, 3H, OCH_3), 3.25 (s, 3H, N-CH_3), 2.25 (s, 3H, C-CH_3). ESI-MS *m/z*: 245 $[M+H]^+$, 267 $[M+Na]^+$, 283 $[M+K]^+$, 511 $[2M+Na]^+$.

*4.1.15. 2-(3-Methoxyphenyl)-5-methyl-1H-pyrrole-3-carboxamide (**19**).*

Compound **19** was prepared according to the procedure used for **15** starting from **13** (300.0 mg, 1.08 mmol), a conc. solution of NH_4OH (18.0 mL) and a catalytic amount of sulphamic acid, maintaining the reaction under stirring for 5 h. Mixture was neutralized by 2N HCl. Aqueous layer was extracted with EtOAc (3 x 10 mL). The combined organic phases were washed with brine, dried over sodium sulfate, filtered and concentrated. Crude was purified by means of flash

chromatography (petroleum ether/EtOAc 5:1) affording the title compound as a pale-yellow oil (20% yield). ^{1}H NMR (300 MHz, $CDCl_3$) δ 8.93 (br s, 1H, pyrrol-NH), 7.27-7.21 (m, 1H, ArH), 7.05 (s, 2H, ArH), 6.82 (d, *J* = 8.7 Hz, 1H, ArH), 6.22 (s, 1H, pyrrol-CH), 5.59 (br s , 2H, $CONH_2$), 3.75 (s, 3H, OCH_3), 2.20 (s, 3H, CH_3). ESI-MS *m/z*: 231 $[M+H]^+$, 253 $[M+Na]^+$.

*4.1.16. 2-(3-Hydroxyphenyl)-5-methyl-1H-pyrrole-3-carboxamide (**20a**).*

To a suspension of **19** (141.0 mg, 0.61 mmol) in dry DCM (10.0 mL), boron tribromide (1 M solution in DCM, 1.8 mL, 1.82 mmol) was added at -78 °C. The reaction mixture was then allowed to warm to 25 °C and stirred for 96 h. Mixture was treated with 4N NaOH and extracted with DCM (3 x 15 mL). The aqueous layers were then acidified to pH = 2 with 6M HCl and extracted with EtOAc. The combined organic extracts were dried over anhydrous sodium sulphate, filtered and concentrated to afford the pure product as an amorphous yellow solid (85% yield). ^{1}H NMR (300 MHz, CD_3OD) δ 7.22-7.14 (m, 1H, ArH), 6.97-6.95 (m, 2H, ArH), 6.72 (dd, *J* = 2.7, 6.6 Hz, 1H, ArH), 6.18 (s, 1H, pyrrol-CH), 2.21 (s, 3H, CH_3). ESI-MS *m/z*: 239 $[M+Na]^+$.

*4.1.17. 2-(3-Hydroxyphenyl)-1,5-dimethyl-1H-pyrrole-3-carboxamide (**20b**).*

Title compound was prepared according to the procedure used for the preparation of **20a** starting from **17** (145.0 mg, 0.59 mmol) and BBr_3 (1M solution in DCM, 1.7 mL, 1.76 mmol). Compound **20b** was obtained as an amorphous pink solid (99% yield). ^{1}H NMR (300 MHz, CD_3OD) δ 7.31 (t, *J* = 6.9 Hz, 1H, ArH), 6.89-6.87 (m, 1H, ArH), 6.80 (d, *J* = 7.5 Hz, 1H, ArH), 6.76-6.75 (m, 1H, ArH), 6.31 (s, 1H, pyrrol-CH), 3.25 (s, 3H, N-CH_3), 2.25 (s, 3H, C-CH_3). ESI-MS *m/z*: 231 $[M+H]^+$, 253 $[M+Na]^+$, 483 $[2M+Na]^+$.

*4.1.18. 3-(3-Carbamoyl-1,5-dimethyl-1H-pyrrol-2-yl)phenyl (2-(4-phenylpiperazin-1-yl)ethyl)carbamate (**5e**).*

Compound **20a** (20.0 mg, 0.07 mmol) was dissolved in H_2O (10.0 mL) and then carbonylimidazolide **8** (15.4 mg, 0.07 mmol) was added. Mixture was stirred at 25 °C for 5 h. The aqueous layer was extracted with EtOAc (3 x 10 mL). The combined organic phases were washeda

saturated solution of NaCl, dried over sodium sulfate, filtered and concentrated. Crude was then triturated with Et_2O to eliminate the 1*H*-imidazole released by the reaction. Silica gel column chromatography (EtOAc 100% to EtOAc/MeOH 20:1) afforded compound **5e** as an amorphous white solid (20% yield). ^{1}H NMR (300 MHz, $CDCl_3$) δ 8.38 (br s, 1H, pyrrol-H), 7.38-7.25 (m, 5H, ArH), 7.10-7.08 (m, 1H, ArH), 6.93 (d, *J* = 7.8 Hz, 2H, ArH), 6.86 (t, *J* = 7.8 Hz, 1H, ArH), 6.28 (s, 1H, pyrrol-CH_2), 5.82 (br s, 1H, OCONH), 5.51 (br s, 2H, $CONH_2$), 3.47-3.40 (m, 2H, CH_2-NH), 3.24-3.21 (m, 4H, Ar-N(CH_2)$_2$ piperazine), 2.68-2.60 (m, 6H, N-(CH_2)$_2$ piperazine), 2.25 (s, 3H, CH_3).^{13}C NMR (75 MHz, $CDCl_3$) δ 167.3, 154,8, 151.4 (2), 133.5, 131.5, 129.9, 129.4 (2), 128.6, 125.8, 122.3, 121.5, 120.1, 116.3 (2), 116.0, 109.0, 57.0, 53.2 (2), 49.3 (2), 37.8, 12.9. ESI-MS *m/z*: 470 [*M*+Na]$^+$. Anal. ($C_{25}H_{29}N_5O_3$) C, H, N.

*4.1.19. 3-(3-Carbamoyl-5-methyl-1H-pyrrol-2-yl)phenyl (2-(4-phenylpiperazin-1-yl)ethyl)carbamate (**5f**).*

Title compound was obtained according to the procedure followed for **5e** (20% yield^{1}H NMR (300 MHz, $CDCl_3$) δ 7.47 (t, *J* = 7.8 Hz, 1H, ArH), 7.30-7.19 (m, 5H, ArH), 6.95-6.92 (m, 2H, ArH), 6.87 (t, *J* = 7.2 Hz, 1H, ArH), 6.44 (s, 1H, pyrrol-CH), 5.69 (br s, 1H, OCONH), 5.10 (br, 2H, $CONH_2$), 3.42 (t, *J* = 5.9 Hz, 2H, CH_2-NH), 3.28 (s, 3H, N-CH_3), 3.24-3.21 (m, 4H, ArN(CH_2)$_2$ piperazine, 2.69-2.61 (m, 6H, N(CH_2)$_2$ piperazine), 2.25 (s, 3H, C-CH_3). ^{13}C NMR (75 MHz, $CDCl_3$) δ 166.7, 154.5, 151.6, 149.2, 133.4, 130.1, 129.7, 129.4, 127.9 (2), 124.7, 122.4, 120.1, 118.6, 116.3, 115.8, 108.2, 56.9, 53.1, 49.3, 37.8, 31.7, 12.6. ESI-MS *m/z*: 462 [*M*+H]$^+$, 484 [*M*+Na]$^+$. Anal. ($C_{26}H_{31}N_5O_3$) C, H, N.

*4.1.20. 2-(5,5-Dimethyl-1,3-dioxan-2-yl)-1-methyl-1H-pyrrole (**22**).*

1-Methyl-1*H*-pyrrole-3-carbaldehyde **21** (931 μL, 9.16 mmol) was dissolved in toluene (56.0 mL). *p*-Toluenesulfonic acid (17.4 mg, 0.09 mmol) and 2,2-dimethylpropane-1,3-diol (1.91 g, 18.33 mmol) were sequentially added. The reaction mixture was refluxed in a Dean-Stark apparatus to remove H_2O from the reaction. The reaction mixture was refluxed for 24 h. A saturated solution of

$NaHCO_3$ was then added to stop the reaction, and toluene was removed under reduced pressure. The aqueous phase was extracted with EtOAc (3 x 10 mL). The combined organic layers were washed with a saturated solution of NaCl, dried over anhydrous sodium sulphate, filtered and concentrated. Crude was purified first by column chromatography on silica gel (petroleum ether/EtOAc 10:1), then by distillation at 110 °C to eliminate the residual aldehyde. Product **22** was obtained as a colorless oil (99%, yield). ^{1}H NMR (300 MHz, $CDCl_3$) δ 6.56-6.55 (m, 1H, pyrrol-CH), 6.22-6.20 (m, 1H, pyrrol-CH), 6.04-6.01 (m, 1H, pyrrol-CH), 5.42 (s, 1H, CH), 3.77 (s, 3H, N-CH_3), 3.74 (s, 2H, CH_2), 3.62 (s, 2H, CH_2), 1.30 (s, 3H, CH_3), 0.79 (s, 3H, CH_3). ESI-MS *m/z*: 391 $[2M+H]^+$, 413 $[2M+Na]^+$, 429 $[2M+K]^+$.

*4.1.21. 2-Bromo-5-(5,5-dimethyl-1,3-dioxan-2-yl)-1-methyl-1H-pyrrole (**23**).*

Compound **22** (954.0 mg, 4.89 mmol) was dissolved in dry THF (12.0 mL); the solution was cooled to -20 °C and NBS (827.2 mg, 4.64 mmol) was added. The reaction mixture was stirred for 16 h, under N_2 atmosphere at -20 °C. Evaporation and silica gel column chromatography (petroleum ether/EtOAc 4:1) afforded the title compound as a crystalline white solid (81% yield). M.p. = 107-108 °C. ^{1}H NMR (300 MHz, $CDCl_3$) δ 6.17 (d, *J* = 4.0 Hz, 1H, pyrrol-CH), 6.04 (d, *J* = 4.0 Hz, 1H, pyrrol-CH), 5.31 (s, 1H, CH), 3.69 (s, 3H, N-CH_3), 3.67 (s, 4H, CH_2), 1.27 (s, 3H, CH_3), 0.79 (s, 3H, CH_3). ESI-MS *m/z*: 275 $[M+H]^+$, 297 $[M+Na]^+$.

*4.1.22. 5-Bromo-1-methyl-1H-pyrrole-2-carbaldehyde (**24**).*

Compound **23** (2.17 g, 7.90 mmol) was dissolved in acetone (7.9 mL) and then 1M HCl (15.8 mL) was added. The reaction mixture was refluxed for 3 h. After cooling to 25 °C, acetone was removed and the aqueous residue was extracted with diethyl ether (3 x 10 mL). The combined organic layers were washed with a saturated solution of NaCl, dried over anhydrous sodium sulphate, filtered and concentrated. Silica gel column chromatography (petroleum ether/EtOAc 10: 1) afforded the title compound as an amorphous white solid (83% yield). ^{1}H NMR (300 MHz, $CDCl_3$) δ 9.35 (s, 1H,

CHO), 6.88 (d, *J* = 4.2 Hz, 1H, pyrrol-CH), 6.32 (d, *J* = 4.2 Hz, 1H, pyrrol-CH), 3.96 (s, 3H, N-CH_3). ESI-MS *m/z*: 189 $[M+H]^+$, 211 $[M+Na]^+$.

*4.1.23. 5-Bromo-1-methyl-1H-pyrrole-2-carbonitrile (**25**).*

To a solution of compound **24** (613.0 mg, 3.28 mmol) in THF (1.0 mL) and conc. NH_4OH (5.2 mL), iodine (1.66 g, 6.56 mmol) was added. The reaction mixture was stirred for 16 h at 25 °C. A saturated solution of $Na_2S_2O_3$ was added to quench the iodine excess and the aqueous layer was extracted with DCM (3 x 10 mL). The combined organic layers were washed with a saturated solution of NaCl, dried over anhydrous sodium sulphate, filtered and concentrated. The crude was purified by means of flash chromatography (petroleum ether/EtOAc 10: 1) to afford the title compound as yellow oil (91% yield). ^{1}H NMR (300 MHz, $CDCl_3$) δ 6.76 (d, *J* = 4.0 Hz, 1H, pyrrol-CH), 6.22 (d, *J* = 4.3 Hz, 1H, pyrrol-CH), 3.73 (s, 3H, N-CH_3). ESI-MS *m/z*: 186 $[M+H]^+$.

*4.1.24. 5-(3-Hydroxyphenyl)-1-methyl-1H-pyrrole-2-carbonitrile (**26**).*

A mixture of compound **25** (100.0 mg, 0.54 mmol) and $Pd(PPh_3)_4$ (31.2 mg, 0.03 mmol) in toluene (3.5 mL), was stirred under N_2 atmosphere for 10 min. at 25 °C. Then a solution of Na_2CO_3 (359.8 mg, 3.39 mmol) in H_2O (1.75 mL) and a solution of 3-hydroxyphenylboronic acid (74.5 mg, 0:54 mmol) in EtOH (1.6 mL) were sequentially added. The resulting mixture was refluxed under N_2 atmosphere for 3 h. Volatiles were removed and the residue was taken up with water and extracted with DCM (3 x 10 mL). The combined organic layers were washed with a saturated solution of NaCl, dried over anhydrous sodium sulphate, filtered and concentrated. Silica gel column chromatography (petroleum ether/EtOAc 5:1) afforded the title compound as an amorphous white solid. ^{1}H NMR (300 MHz, $CDCl_3$) δ 7.33-7.26 (m, 1H, ArH), 6.93-6.89 (m, 3H, ArH), 6.85 (d, *J* = 3.6 Hz, 1H, ArH), 6.22-6.20 (m, 2H, pyrrol-CH), 3.73 (s, 3H, N-CH_3). ESI-MS *m/z*: 197 $[M-H]^-$, 199 $[M+H]^+$, 221 $[M+Na]^+$.

*4.1.25. 5-(3-Hydroxyphenyl)-1-methyl-1H-pyrrole-2-carboxamide (**27**).*

Title compound was prepared according to the procedure described for **11**, starting from compound **26** (100.0 mg, 0.50 mmol), 6M NaOH (1.7 mL) and 30% aqueous H_2O_2 (1.70 mL). Crude was purified by flash chromatography on silica gel (petroleum ether/EtOAc 1: 2) to obtain pure compound **27** as an amorphous pink solid (67% yield). ^{1}H NMR (300 MHz, acetone-d_6) δ 8.68 (br, 1H, OH), 7.27 (t, *J* = 7.8 Hz, 1H, ArH), 7.05-6.40 (m, 2H, Ar), 6.93-6.88 (m, 3H, Ar), 6.86 (d, *J* = 1.65, 1H, pyrrol-CH), 6.13 (d, *J* = 3.9 Hz, 1H, pyrrol-CH), 3.88 (s, 3H, N-CH_3). ESI-MS *m/z*: 217 $[M+H]^+$, 239 $[M+Na]^+$, 255 $[M+K]^+$.

*4.1.26. 3-(4-Carbamoyl-1H-1,2,3-triazol-1-yl)phenyl (2-(4-phenylpiperazin-1-yl)ethyl)carbamate (**5g**).*

Title compound was prepared according to the procedure described for **5c** starting from **27** (30.0 mg, 0.14 mmol), phosgene (20% solution in toluene, 146 μL, 0.28 mmol), DMAP (67.2 mg, 0.55 mmol) and amine **7a** (56.8 mg, 0.28 mmol). The solvent was removed and the crude was purified by means of column chromatography on silica gel (100% EtOAc). Title compound **5g** was obtained as a colorless transparent oil (30% yield). ^{1}H NMR (300 MHz, $CDCl_3$) δ 7.41 (t, *J* = 7.8 Hz, 1H, ArH), 7.30-7.25 (m, 3H, ArH), 7.17 (t, *J* = 9.6 Hz, 2H, ArH), 6.94 (d, *J* = 7.8 Hz, 2H, ArH), 6.87 (t, *J* = 7.2 Hz, 1H, ArH), 6.66 (d, *J* = 4.2 Hz, 1H, pyrrol-CH), 6.18 (d, *J* = 3.9 Hz, 1H, pyrrol-CH), 5.71 (br s, 1H, OCONH), 5.52 (br s, 2H, $CONH_2$), 3.89 (s, 3H, N-CH_3), 3.47-3.41 (m, 2H, CH_2-NH), 3.25-3.23 (m, 4H, ArN-$(CH_2)_2$ piperazine), 2.70-2.62 (m, 6H, N$(CH_2)_2$ piperazine, N-CH_2). ^{13}C NMR (75 MHz, $CDCl_3$) δ 163.8, 154.7, 151.4, 151.3, 140.1, 133.6, 129.6, 129.4, 126.4, 126.2, 122.8, 121.4, 120.2, 116.4, 113.2, 109.0, 57.0, 53.2, 49.3, 37.8, 34.8. ESI-MS *m/z*: 448 $[M+H]^+$, 470 $[M+Na]^+$. Anal. ($C_{25}H_{29}N_5O_3$) C, H, N.

*4.1.27. 1-Azido-3-methoxybenzene (**29**).*

In a sealed tube, 1-bromo-3-methoxybenzene **28** (100.0 mg, 0.53 mmol), NaN_3 (69.5 mg, 1.07 mmol), CuI (10.2 mg, 0.05 mmol) and *L*-proline (18.5 mg, 0.16 mmol) were sequentially dissolved in a mixture of EtOH/H_2O = 7/3 (740.0 μL of EtOH and 320.0 μL of H_2O). Mixture was then

refluxed for 16 h. After cooling to 25 °C, EtOH was evaporated and the aqueous layer was extracted with EtOAc (3 x 10 mL). The combined organic phases were dried over anhydrous Na_2SO_4, filtered and concentrated. Crude was purified by means of flash chromatography (100% petroleum ether) to give compound **29** as pale-yellow oil (47% yield). ^{1}H NMR (300 MHz, CD_3OD) δ 7.25 (t, *J* = 8.4 Hz, 1H, ArH), 6.70 (d, *J* = 8.4 Hz, 1H, ArH), 6.62 (d, *J* = 8.4 Hz, 1H, ArH), 6.55-6.53 (m, 1H, ArH), 3.76 (s, 3H, OCH_3). ESI-MS *m/z*: 137 $[M+H]^+$, 160 $[M+Na]^+$, 176 $[M+K]^+$.

*4.1.28. Methyl 1-(3-methoxyphenyl)-1H-1,2,3-triazole-4-carboxylate (**30**).*

Compound **29** (20.0 mg, 0.13 mmol) and methyl propiolate (11.3 mg, 0.13 mmol) were dissolved in dry THF (2.0 mL). DIPEA (117 µL, 0.67 mmol) and CuI (5.1 mg, 0.03 mmol) were sequentially added. The reaction mixture was stirred at 25 °C for 12 h. Evaporation and silica gel column chromatography (petroleum ether/EtOAc 6:1) afforded **30** as an amorphous white solid (99% yield). ^{1}H NMR (300 MHz, $CDCl_3$) δ 8.50 (s, 1H, triazol-CH), 7.42 (t, *J* = 8.4 Hz, 1H, ArH), 7.34-7.33 (m, 1H, ArH), 7.28-7.25 (m, 1H, ArH), 7.00 (dd, *J* = 2.4, 8.4 Hz, 1H, OH), 3.98 (s, 3H, OCH_3), 3.87 (s, 3H, $COOCH_3$). ESI-MS *m/z*: 234 $[M+H]^+$, 256 $[M+Na]^+$, 489 $[2M+Na]^+$.

*4.1.29. 1-(3-Methoxyphenyl)-1H-1,2,3-triazole-4-carboxylic acid (**31**).*

Compound **30** (30.0 mg, 0.13 mmol) was dissolved in EtOH (2.4 mL) and H_2O (0.8 mL), and NaOH (129.7 mg, 3.24 mmol) was added. Mixture was refluxed for 16 h. After evaporation of EtOH, the residue was taken up with water, acidified with 2N HCl until pH = 1 and extracted with EtOAc (3 x 10 mL). The combined organic phases were dried over anhydrous Na_2SO_4, filtered and concentrated to give the title compound as pure amorphous brown solid (40% yield). ^{1}H NMR (300 MHz, CD_3OD) δ 9.08 (s, 1H, triazol-CH), 7.52-7.47 (m, 3H, ArH), 7.08 (d, *J* = 7.5 Hz, 1H, ArH), 3.89 (s, 3H, $COOCH_3$). ESI-MS *m/z*: 220 $[M+H]^+$.

*4.1.30. 1-(3-Hydroxyphenyl)-1H-1,2,3-triazole-4-carboxamide (**32**).*

1-*(3-Methoxyphenyl)-1H-1,2,3-triazole-4-carboxamide.* Compound **31** was dissolved in dry THF and the mixture cooled down to -10 °C. *N*-methylmorpholine (25 µL, 0.23 mmol) and isobutyl

chloroformate (30 µL, 0.23 mmol) were sequentially added. After formation of a suspension, conc. NH_4OH (40 µL, 0.34 mmol) was added. The reaction mixture was stirred under N_2 atmosphere for 30 min at -10 °C and for an additional 1 h at 25 °C. Solvent was removed and the residue was taken up with water and extracted with EtOAc (3 x 10 mL). The combined organic phases were dried over anhydrous Na_2SO_4, filtered and concentrated to afford 1-*(3-methoxyphenyl)-1H-1,2,3-triazole-4-carboxamide* in quantitative yield. ^{1}H NMR (300 MHz, $CDCl_3$) δ 8.52 (s, 1H, triazol-CH), 7.45 (t, *J* = 8.1 Hz, 1H, ArH), 7.35-7.25 (m, 2H, ArH), 7.11 (br s, 1H, $CONH_2$), 7.04-7.01 (m, 1H, ArH), 5.71 (br s, 1H, $CONH_2$), 3.89 (s, 3H, $COOCH_3$). ESI-MS *m/z*: 219 $[M+H]^+$, 241 $[M+Na]^+$.

Compound **32** was prepared according to the procedure used for **20a** starting from 1-*(3-methoxyphenyl)-1H-1,2,3-triazole-4-carboxamide* (200.0 mg, 0.92 mmol) and BBr_3 (1 M solution in DCM, 5.4 mL, 5.40 mmol). Title compound was obtained as an amorphous white solid enough pure to be used in the next step without any further purification (45% yield). ^{1}H NMR (300 MHz, CD_3OD) δ 8.82 (s, 1H, triazol-CH), 7.40-7.35 (m, 1H, ArH), 7.30-7.27 (m, 2H, ArH), 6.94-6.90 (m, 1H, ArH). ESI-MS *m/z*: 205 $[M+H]^+$, 227 $[M+Na]^+$.

*4.1.31. 3-(5-Carbamoyl-1-methyl-1H-pyrrol-2-yl)phenyl (2-(4-phenylpiperazin-1-yl)ethyl)carbamate (**5h**).*

Compound **5h** was synthesized following the same procedure described for **5c** starting from **32** (20.0 mg, 0.09 mmol), phosgene (20% solution in toluene, 100 µL, 0.10 mmol), DMAP (47.6 mg, 0.39 mmol) and amine **7a** (38.9 mg, 0.19 mmol). Crude was purified by silica gel column chromatography (100% EtOAc to EtOAc/MeOH 100:1) affording title compound as an amorphous white solid (20% yield). ^{1}H NMR (300 MHz, DMSO) δ 9.26 (s, 1H, triazole-CH), 7.98 (br s, 1H, OCONH), 7.86-7.75 (m, 3H, ArH), 7.59 (t, *J* = 8.4 Hz, 2H, ArH), 7.26 (dd, *J* = 3.0, 8.4 Hz, 1H, ArH), 7.18 (t, *J* = 7.5 Hz, 2H, ArH), 6.91 (d, *J* = 8.1Hz, 2H, ArH), 6.75 (t, *J* = 7.2 Hz, 1H, ArH), 3.35-3.22 (m, 2H, CH_2-NH), 3.13-3.10 (m, 4H, ArN-$(CH_2)_2$ piperazine), 2.57-2.54 (m, 6H, N-$(CH_2)_2$, pipeazine, N-CH_2). ^{13}C NMR (75 MHz, DMSO) δ 161.9, 159.1, 151.7, 149.0, 144.4, 138.0,

131.5, 129.6, 125.4, 119.4, 116.7, 116.0, 111.5, 108.0, 58.6, 53.4, 48.8, 37.3. ESI-MS *m/z*: 436 $[M+H]^+$, 458 $[M+Na]^+$. Anal. ($C_{22}H_{25}N_7O_3$) C, H, N.

4.2 Computational Studies

4.2.1. Docking studies

Molecules preparation. Three-dimensional structures of all compounds in this study were built by means of Maestro (Maestro, version 10.3, Schrödinger LLC, New York, NY, 2015) applying the previously adopted protocol.[26, 28, 49]

Proteins preparation. The three-dimensional structures of: FAAH enzyme (PDB ID: 3PPM[50]), dopamine D_2 (PBD ID: 6CM4[51]) and D_3 (PDB ID: 3PBL[52]) receptors were taken from the PDB and imported into Schrödinger Maestro molecular modeling environment. Water molecules and compounds used for the crystallization were removed from the available experimental structures. The obtained enzymes were submitted to protein preparation wizard implemented in Maestro suite 2015 as reported.[22,24,[53]]

Molecular docking .Molecular docking was carried out using the Schrödinger suite 2015 by applying the IFD protocol as previously reported.[22,24,[53]] This procedure induces conformational changes in the binding site to accommodate the ligand and exhaustively identify possible binding modes and associated conformational changes by side-chain sampling and backbone minimization. The protein and the ligands used were prepared as reported in the previous paragraphs. The boxes for docking calculation were built taking into account the centroid of the co-crystallized ligands for all enzymes. Complexes within 30.0 kcal/mol of minimum energy structure were taken forward for redocking. The Glide redocking stage was performed by XP (Extra Precision) methods. The calculations were performed using default IFD protocol parameters. No hydrogen bonding or other constraints were used. For dopamine receptors we selected the use of implicit membrane in the Prime refinement step in order to obtain more reliable results. The membranes were placed

according to the residues in the transmembrane domain of dopamine D_2 receptor (UniProt ID: P14416) and dopamine D_3 receptor (UniProt ID: P00720) as found in UniProtKB database. The selected IFD docking protocol was able to correctly accommodate the co-crystallized ligands, belonging to the proteins used in this study (data not shown).

4.2.2 Molecular Properties Prediction

The *in silico* drug-like features of the designed compounds were evaluated by means of: i) QikProp implemented in Maestro suite (QikProp, version 4.3, Schrödinger, LLC, New York, NY, 2015) for the assessment of the compounds physico-chemical properties; ii) 3D-chERGi, an in-house 3D-QSAR model for predicting *h*ERG K^+ channel affinity).[54] The outputs of these calculations are reported in Table S1.

4.2.3. P450 site of metabolism

Compounds **3a** and **5c** were evaluated for their potential sites of metabolism by P450 site of metabolism (P450 SOM) workflow implemented in Schrödinger suite 2018. For each molecule P450 SOM performed a calculation of intrinsic reactivity coupled to IFD for the selected isoform of cytochrome. The reactivity rules have been parametrized in P450 SOM to predict atomic reactivity profiles for promiscuous P450 enzymes that are thought to be mostly independent of structural restrictions on the binding poses. The reactivity is predicted with a linear free energy approach based on the Hammett and Taft scheme, where the reactivity of a given atom is the sum of a baseline reactivity rate and a series of perturbations determined by the connectivity. The IFD approach is a variation on the normal protocol. The initial sampling is enhanced by generating multiple starting conformations, so that a wider range of poses is found in the initial docking stage. The initial docking includes van der Waals scaling of the receptor and alanine mutation of the most flexible residues. In the Prime refinement step, any residue with an atom within 5 Å of any ligand pose is selected for side-chain prediction. The subsequent minimization includes the ligand, side chains, and backbones of the flexible residues. The ligand is then redocked into each of the low-

energy protein conformations, determined by a 40 kcal/mol cut-off. There is no final scoring stage, because all poses are considered in determining which atoms are sufficiently accessible to the reactive heme iron. Any atom within the cut-off distance of 5 Å from the heme iron is considered as a potential site of metabolism.[55]

4.3. Solubility and chemical stability studies

*HPLC analysis of compounds **3a** and **5c***. For the HPLC analysis a Chromolith HPLC column RP-18 was employed. The runs were performed by a gradient elution starting from a mixture 20% MeCN (0.1 % TFA as phase modifier) in H_2O (0.1% TFA as phase modifier) to 70% MeCN (0.1% TFA) in H_2O (0.1 % TFA) in 15 min. The flow speed was settled at 1.0 mL/min and the temperature was maintained at 25 °C. The volume of injection of the sample was of 10 µL and the wavelength selected for the detection was 254 nM. The retention times obtained following this protocol for compounds **3a** and **5c** were 12.8 min and 6.58 min, respectively.

Solubility Assay and chemical stability at 25 °C. A stock solution for each tested compound was prepared dissolving the sample in DMSO to a final concentration of 10 mM. From the stock solution, three samples were prepared: one was used as the standard solution and the other two as the test solutions at pH 3.0 and pH 7.4. The samples' concentration of these solutions was 250 µM with a DMSO content of 2.5 % (v/v).

The standard solution was prepared by dilution of the stock solution in PBS-buffer solution (MeCN/water, 60:40); the dilution of the stock solution in 50 mM acetic acid afforded the samples' solution at pH 3.0; and the dilution of the stock solution in 50 mM aqueous PBS-buffer afforded the samples' solution at pH 7.4. These suspension/solutions were sealed and left for 24 h at 25 °C under orbital shaking to achieve "pseudothermodynamic equilibrium". After that time the solutions were filtered using PTFE filters and successively diluted 1:2 with the buffer solution used for the preparation of the samples. Then they were analyzed by HPLC/UV/DAD, using UV detection at

254 nm for quantitation. Solubility was calculated by comparing areas of the sample and of the standard:

$$S = \frac{Asmp \times FD \times Cst}{Ast}$$

S = solubility of the compound (μM); Asmp = UV area of the sample solution; FD = dilution factor (2); Cst = standard concentration (250 μM); Ast = UV area of the standard solution.

For each sample the analysis was performed in triplicate and the solubility result reported was obtained from the average of the three values.

The same sample solutions were prepared to evaluate the chemical stability of the compounds after 24 h at 25 °C and analyzed by HPLC/UV/DAD, using UV detection at 254 nm for quantitation. Stability was calculated by comparing the area of the peak at T_0 and the area of the peak of the same solution after 24 h. A stability percentage value was calculated by this method at pH 3.0 and pH 7.4 for each compound by applying the following formula:

$$\%_{remaining} = \frac{Ac_{24}}{Ac_{T_0}} \times 100$$

Ac_{24} = area of the sample after 24 h at 25 °C; Ac_{T0} = area of the sample at T_0.

For each sample the analysis was performed in triplicate and the stability result reported was obtained from the average of the three values.

4.4. Biological Data

4.4.1. Enzymatic assays.

4.4.1.1. FAAH activity assay.

FAAH activity was assayed in mouse brain incubated with 10 μM [^{14}C]AEA (ARC, St. Louis, MO, USA) at 37 °C for 15 min (pH 9.0). The reaction was stopped with a 2:1 (v/v) mixture of chloroform/methanol, and the release of [^{14}C]ethanolamine in the aqueous phase was measured as

reported.[56] Control experiments were also carried out in the presence of the selective FAAH inhibitor **1a**. The effect of different compounds on FAAH activity was ascertained by adding each substance directly to the incubation medium.

4.4.1.2. MAGL activity assay.

Mouse brain was thawed and homogenized at 4 °C in sodium phosphate buffer (50 mM, pH = 8.0) containing 0.32 M sucrose. Homogenates were centrifuged at 4 °C sequentially at 800x*g*, 10,000x*g*, and 100,000*x*g. MAGL activity was assayed in final tissue supernatants, incubated with 10 μM [^{3}H]2-OG (20 Ci/mmol; ARC, St. Louis, MO) at 37 °C for 30 min.[56] The reaction was stopped with a 2:1 (v/v) mixture of chloroform/methanol and the release of [^{3}H]glycerol in the aqueous phase was measured by scintillation counting.

4.4.2. Receptor binding assays

4.4.2.1. CB_1R and CB_2R assays.

Mouse brain was resuspended in 2 mM Tris–EDTA, 320 mM sucrose, 5 mM $MgCl_2$ (pH 7.4), then it was homogenized in a Potter homogenizer and centrifuged three time at 1000x*g* (10 min each), and the pellet was discharged. The supernatant was centrifuged at 18000x*g* (30 min), and the pellet was resuspended in assay buffer (50 mM Tris–HCl, 2 mM Tris–EDTA, 3 mM $MgCl_2$, pH 7.4).[56] These membrane fractions were used in rapid filtration assays with radiolabel agonist [^{3}H]CP55,940 (Perkin-Elmer Life Sciences, Boston, MA, USA). In all experiments, nonspecific binding was determined in the presence of 1 μM "cold" agonist, and the effect of selective compounds for CB_1R or CB_2R was tested by adding each substance directly to the incubation medium.

4.4.2.2. Dopamine D_2 and D_3 receptor assays.

CHO-hD_3 and CHO-hD_2 Membrane Preparation. The frozen pellet of cells recombinantly expressing *h*D_3 and *h*D_2-Gα16-CHO receptors was thawed and homogenized in 10 volumes (w/v) in Membrane Preparation Buffer 1 using an Ultraturrax (3 times for 10 s each cycle). The homogenate was centrifuged for 20 min, 4 °C, at 18500 rpm (40000 rcf) in a SL-50T Sorvall rotor and the pellet resuspended in 10 volumes w/v in Membrane Preparation Buffer 1 and rehomogenized as before. After centrifugation, the pellet was resuspended in 5 volumes of Membrane Preparation Buffer 2. The resulting suspension was aliquoted and frozen down at −80 °C. Protein concentration was determined according to the instructions provided within the BioRad reagent using a BSA standard curve (Buffer 1 = HEPES 20 mM, EDTA 2 mM pH = 7.4, ice cold; Buffer 2 = HEPES 20 mM pH = 7.4, NaCl 100 mM, $MgCl_2$ 10 mM, EDTA 1 mM, ice cold).

Competition Binding Experiments at hD_2 receptors. Competition binding experiments were performed in a 96-deep-well plate at room temperature (23 °C) with a final assay volume of 1000 μL/well, according to the following protocol: 800 μL of binding buffer were dispensed into each well of the compound plate. [^{3}H]-Spiperone stock was diluted in binding buffer solution to obtain the 10× [^{3}H]-spiperone solution (0.8 nM). Then 100 μL of 0.8 nM [^{3}H]-spiperone solution were dispensed into each well of the compound plate. The competition reaction was started by adding 100 μL of *h*D_2-Gα16-CHO membrane suspension in binding buffer. The final membrane concentration/well was 2 μg, and the final [^{3}H]-spiperone concentration was 0.08 nM. The plate was then incubated on a shaker at 23 °C for 120 min. The reaction was terminated by rapid filtration through Unifilter-96 GF/B filter plates presoaked for at least 1 h in polyethylenimine (PEI) 0.5% (w/v) solution and washed with 1.0 mL of ice cold 0.9% NaCl before the filtration using a Packard Cell Harvester. The filter plate was washed 4 times with 1.0 mL of ice-cold 0.9% NaCl and then left to dry for at least 1 h at 40 °C. The plate was sealed with a back-seal; 50 μL of Microscint-20 were added to each well, and the plate was sealed with a top-seal. Bound radioactivity was measured using a Microplate Top-Count. Radioligand concentration was determined as follows: 100 μL of

[^{3}H]-spiperone solution (5×) and 3 mL of Filter Count were mixed in the total added vial and read in β-Counter TriCarb 2900.

Saturation Binding Experiments at hD_2 receptors. Saturation binding experiments were performed similarly to the competition binding experiments, with the following deviation: [^{3}H]-spiperone concentrations were chosen from 0.011 to 3.0 nM in a concentration–response curve with 12 points. The reaction was terminated by rapid filtration through GF/B paper filter presoaked for 1 h in polyethylenimine (PEI) 0.5% (w/v) solution and washed with 1.0 mL of ice-cold 0.9% NaCl before the filtration using a Brandel harvester. The filter was washed 4 times with 1.0 mL of ice-cold 0.9% NaCl. The filter was put into a pico-vial (PerkinElmer 600252), and 4 mL of Filter Count were added. Bound radioactivity was measured using a β-Counter. Samples of working radioligand solution were taken and measured by traditional liquid scintillation counting in order to determine the actual concentration of radiolabel added.

Competition Binding Experiments at hD_3 receptors. Competition binding experiments were performed in a 96-deep well plate at room temperature (23 °C) with a final assay volume of 500 μL/well according to the following protocol: (a) 300 μL of binding buffer were dispensed into each well of the compound plate; (b) [^{3}H]-spiperone stock was diluted in binding buffer solution to obtain the 5× [^{3}H]-spiperone solution (1.5 nM); (c) 100 μL of 1.5 nM [^{3}H]-spiperone solution were dispensed into each well of the compound plate; (d) the competition reaction was started by adding 100 μL of *h*DRD$_3$-CHO membrane suspension in binding buffer. The final membrane concentration/well was 3.5 μg, and the final [^{3}H]-spiperone concentration was 0.3 nM. The plate was then incubated on a shaker at 23 °C for 90 min. The reaction was terminated by rapid filtration through Unifilter-96 GF/B filter plates presoaked for 1 h in polyethylenimine (PEI) 0.5% (w/v) solution and washed with 1.0 mL of ice-cold 0.9% NaCl before the filtration using a Packard Cell Harvester. The filter plate was washed 4 times with 1.0 mL of ice-cold 0.9% NaCl and then left to dry for at least 1 h at 40 °C. The plate was sealed with a back-seal; 50 μL of Microscint-20 were

added to each well, and the plate was sealed with a top-seal. Bound radioactivity was measured using a Microplate TopCount. Radioligand concentration was determined as follows: 100 μL of [^{3}H]-spiperone solution (5×) and 3 mL of Filter Count were mixed in the total added vial and read in β-Counter TriCarb 2900.

Saturation Binding Experiments at hD_3 receptors. Saturation binding experiments were performed similarly to the competition binding experiments, with the following deviation: [^{3}H]-spiperone concentrations were chosen from 0.015 to 4.0 nM in a concentration response curve with 12 points. The reaction was terminated by rapid filtration through GF\B paper filter presoaked for 1 h in polyethylenimine (PEI) 0.5% (w/v) solution and washed with 1.0 mL of ice-cold 0.9% NaCl before the filtration using a Brandel harvester. The filter was washed 4 times with 1.0 mL of ice-cold 0.9% NaCl. The filter was put into a pico-vial (PerkinElmer 600252), and 4 mL of Filter count were added. Bound radioactivity was measured using a β-Counter. Samples of working radioligand solution were taken and measured by traditional liquid scintillation counting in order to determine the actual concentration of radiolabel added.

4.4.3. Measure of the effect on hERG channel by tail current recording using in vitro rapid ICE.

The potency of the compounds in inhibiting human ERG potassium channel (*h*ERG) tail current was assessed in a recombinant HEK293 cell line stably transfected with *h*ERG cDNA under an inducible promoter, using Rapid ICE (rapid ion channel electrophysiology) assay. Rapid ICE is an automated patch-clamp assay utilizing the QPatch HTX system (Sophion Bioscience A/S). Briefly, inducible HEK *h*ERG cells were cultivated in minimum essential medium supplemented with 10% FBS, 1% nonessential amino acids, 1% sodium pyruvate, 2 mM l-glutamine, 15 μg/mL blasticidin, and 100 μg/mL hygromycin. *h*ERG channel expression induction was obtained by adding 10 μg/mL tetracycline for 24, 48, or 72 h before recordings.

On the day of the experiment, cells were detached with TrypLE and prepared to be loaded on the instrument. Cells were resuspended in 7 mL of Serum-Free Media containing 25 mM Hepes and soybean trypsin inhibitor and immediately placed in the cell storage tank of the machine. The composition of the extracellular buffer was (mM): NaCl 137, KCl 4, $CaCl_2$ 1.8, $MgCl_2$ 1.0, *d*-glucose 10, *N*-2-hydroxyethylpiperazine-*N*′-2-ethanesulfonic acid (HEPES) 10, pH 7.4 with 1 M NaOH. The composition of the pipet solution was (mM): KCl 130, $MgCl_2$ 1.0, ethylene glycol-bis(β-aminoethyl ether)-*N*,*N*,*N*′,*N*′-tetraacetic acid (EGTA) 5, MgATP 5, HEPES 10, pH 7.2 with 1 M KOH. The voltage protocol included the following steps: step from −80 to −50 mV for 200 ms, +20 mV for 4.8 s, step to −50 mV for 5 s, then step to the holding potential of −80 mV. Compounds were dissolved in DMSO and diluted in extracellular buffer to achieve final test concentrations (0.1, 1, and 10 μM) in 0.1% DMSO. The voltage protocol was run and recorded continuously during the experiment. The vehicle, corresponding to 0.1% DMSO in extracellular buffer was then applied for 3 min, followed by the test substance in triplicate. The standard combined exposure time was 5 min. The average of tail current amplitude values recorded from four sequential voltage pulses was used to calculate for each cell the effect of the test substance by calculating the residual current (% control) compared with vehicle pretreatment. Data were reported as % inhibition for each concentration tested, and IC_{50} values were estimated using QPatch software. At least two cells were tested, and even more if results diverged.

4.5. Cytotoxicity and mutagenicity assays.

Materials. Dulbecco's Modified Eagle's Medium, trypsin solution, and all the solvents used for cell culture were purchased from Lonza (Switzerland). Mouse immortalized fibroblasts NIH3T3 and U-373-MG human glioblastoma astrocytoma were purchased from American Type Culture Collection (USA). The mutagenicity assay was supplied by Biologik s.r.l. (Trieste, Italy).

Cell cultures and cytotoxicity assay. NIH3T3 and U-373-MG were utilised for cytotoxicity experiments. Cells were maintained in DMEM at 37 °C in a humidified atmosphere containing 5%

CO_2. The culture media were supplemented with 10% fetal calf serum (FCS), 1% *L*-glutamine-penicillin-streptomycin solution, and 1% MEM Non-Essential Amino Acid Solution. Once at confluence, cells were washed with PBS 0.1 M, taken up with trypsin-EDTA solution and then centrifuged at 1000 rpm for 5 min. The pellet was re-suspended in medium solution (dilution 1:15). The stock solution for each compound was prepared in pure DMSO and diluted with complete culture medium. The solution/suspension obtained was then added to the cell monolayer. Cell viability after 24 h of incubation with the different concentrations of each test compound was evaluated by Neutral Red Uptake by the procedure previously reported.[57] The data processing included the Student's *t* test with $p<0.05$ taken as significance level.

First, the following solutions were prepared in order to determine the percentage of viable cells:

1. Neutral Red (NR) Stock Solution: 0.33 g NR Dye powder in 100 mL sterile H_2O

2. NR Medium: 1.0 mL NR Stock solution + 99.0 Routine Culture Medium pre-warmed to 37 °C

3. NR Desorb solution: 1% glacial acetic acid solution + 50% ethanol + 49% H_2O

At the end of the incubation the routine culture medium was removed from each well, and cells were carefully rinsed with 1 mL of pre-warmed D-PBS. Multiwells were then gently blotted with paper towels. 1.0 mL of NR Medium was added to each well and further incubated at 37 °C, 95% humidity, 5.0% CO_2 for 3 h. The cells were checked during the NR incubation for NR crystal formation. After incubation, the NR Medium was removed; cells were carefully rinsed with 1 mL of pre-warmed D-PBS. Then, the PBS was decanted and blotted from the wells and exactly 1 mL of NR Desorb solution was added to each sample. Multiwells were then put on a shaker for 20-45 min to extract NR from the cells and form a homogeneous solution. During this step the samples were covered in order to protect them from light. After 5 min from the plate shaker removal the absorbance was read at 540 nm by a UV/visible spectrophotometer (Lambda 25, Perkin Elmer).

Mutagenicity assay: Ames test. The TA100 and TA98 strains of *Salmonella Typhimurium* and S9 fraction were utilized for mutagenicity assay. Approximately 10^7 bacteria were exposed to 6 concentrations of each test compound, as well as a positive and a negative control, for 90 min in medium containing sufficient histidine to support approximately two cell divisions. After 90 min, the exposure cultures were diluted in pH indicator medium lacking histidine, and aliquoted into 48 wells of a 384-well plate. Within two days, cells which had undergone the reversion to *His* grew into colonies. Metabolism by the bacterial colonies reduced the pH of the medium, changing the colour of that well. This colour change can be detected visually or by microplate reader. The number of wells containing revertant colonies were counted for each dose and compared to a zero dose control. Each dose was tested in six replicates. The test was performed both with and without S9 fraction.

4.7. Analysis of in vitro metabolic stability of 3a and 5c in human and liver microsomes.

The tested compound (**3a** or **5c**), dissolved in MeCN, was incubated at 37 °C, at 5 μM concentration in 100 mM phosphate buffer (pH 7.4) with 0.3 mg/mL rat and human microsomal preparations as previously reported.[58] Enzymatic reactions were started by addition of a NADPH-regenerating system (2 mM NADPH), 66 mM glucose-6-phosphate, 0.4 U/mL glucose-6-phosphate dehydrogenase in 66 mM $MgCl_2$). Reactions were terminated at regular time intervals (overall range 0-60 min) by adding a 1 mL of MeCN. All incubations were performed in triplicate. HPLC analysis was performed on Agilent 1100 Series liquid chromatography system equipped with a EC 150/4.6 nucleosil 100-3 C18 (Macherey-Nagel) and coupling with UV-VIS detector, setting at λ 254 nm. Analysis was carried out using gradient elution of a binary solution; eluent A was MeCN (MeCN containing 0.1% formic acid), while eluent B consisting of an aqueous solution of formic acid (0.1%). The analysis started at 20% A for three minutes, then rapidly increased up to 90% in 15 min and finally remaining at 90% A until 25 min. The analysis was performed at flow rate of 0.8

mL min^{-1} and injection volume was 20 µL. The intrinsic clearance (Clint) was calculated by the equation:

Clint = k(min-1)x [V]/[P]

where k is the rate constant for the depletion of substrate, V is the volume of incubation in µL and P is the amount of microsomal proteins as reported elsewhere.[59]

4.8. Anti-inflammatory properties evaluation on IMR 32cell line.

Cell culture and treatments. IMR 32 cells line (obtained from American Type Culture Collection, ATCC), were cultured in EMEM medium supplemented with 10% fetal bovine serum (Lonza, Milan, Italy) supplemented with 10% fetal bovine serum (FBS, EuroClone, Milan, Italy), 1% of L-glutamine (Lonza, Milan, Italy) and 1% of penicillin/streptomycin antibiotics (Lonza, Milan, Italy) at 37 °C in 5% CO_2.[60]

The different formulations (**3a** and **5c**) were dissolved in DMSO at the final concentration of 10 mM. Stock solutions were then diluted with cell culture medium, EMEM with Earle's Balanced Salt Solution, in order to obtain an intermediate dose solution (100 µM), to be used for the further dilutions (50 µM, 10 µM, 5 µM, 1 µM, 0.5 µM and 0.1 µM). Control vehicle was represented by DMSO ranging from 0.5% to 0.001%. LPS form Escherichia coli serotype 0111:B4 was purchased from Sigma (St. Louis, MO) and it was dissolved in phosphate buffered saline for use

Cytotoxicity determination. IMR 32 cells were seeded 100,000 cells/well in 96-wells plate and were grown to confluence, then were treated with the mentioned substances in EMEM medium supplemented with 1% fetal bovine serum. The effects of tested compounds on cellular morphology were checked after 24 h using a built-in camera in an inverted Nikon Eclipse microscope (20X magnification).[61] Cytotoxicity was determined by LDH release in the media, as previously reported.[61] All tests were performed at least in triplicate. The absorbance measured from three

wells was averaged, and the percentage of LDH released was calculated as arbitrary unit of change relative to 1% Triton X-100 treated cells.

Nuclear proteins extraction. After treatments with compounds **3a** and **5c** at 0.5 and 1 μM doses for 24 h, cells were challenged with 100 μg/mL LPS for 30 min. Then, cells were detached, washed with ice-cold PBS 1X and cell pellets were resuspended in hypotonic buffer containing 10 mmol/L HEPES (pH 7.9), 10 mmol/L KCl, 1.5 mmol/L $MgCl_2$, 0.3% Nonidet P-40, 0.5 mmol/L dithiothreitol, 0.5 mmol/L phenylmethylsulphonyl fluoride and protease and phosphatase inhibitor cocktails. The lysates were incubated for 15 min on ice with intermitted mixing and then centrifuged at 24500 x g for 15 min at 4 °C, as previously described.[62] The supernatant containing the cytosolic proteins was removed and pellet containing the nuclei were suspended in extraction buffer containing 20 mmol/L HEPES (pH 7.9), 0,6 mol/L KCl, 1.5 mmol/L $MgCl_2$, 20% glycerol, 0.5 mmol/L phenylmethylsulphonyl fluoride and protease and phosphatase inhibitor cocktails and then incubated for 30 min on ice with intermitted mixing. Samples were centrifuged at 21100 x g for 15 min to obtain supernatants containing nuclear fractions. Protein concentration was determined by Bradford analysis (Biorad protein assay; Biorad, Milan, Italy).

NF-κB nuclear translocation. NF-κB DNA-binding capability was evaluated using "TransAM NF-κB" ELISA kit (Active Motif, USA). Nuclear protein extracts from treated IMR 32 cells were incubated with NF-κB consensus oligonucleotides (5′-GGG ACT TTCC-3′) immobilized on 96-well plate for 1 h at rt. A secondary antibody conjugated with a horseradish peroxidase provides a colorimetric output, spectrophotometrically detected at 450 nm.

Western blot analysis. After protein quantification, 40 μg boiled proteins were loaded into 10% sodium dodecyl sulphate-polyacrylamide electrophoresis gels and separated by molecular size. Gels were electro-blotted onto nitrocellulose membranes and then blocked for 90 min in Tris-buffered saline, pH 7.5, containing 0.5% Tween 20 and 5% (w/v) skim milk powder. Membranes were incubated overnight at 4 °C with the appropriate primary antibody: anti-NF-κB, p65 subunit, diluted

1:1000 (Millipore, Billerica, Massachusetts). The membranes were finally incubated with the peroxidase-conjugated secondary anti-Rabbit antibody (1:5000) for 1 h. The bound antibodies were detected by chemiluminescence (Biorad, Milan, Italy). β-Actin or Lamin A were used as loading controls. Images of the bands were digitized using an Epson Stylus SX405 scanner and the densitometry analysis was performed using Image-J software.

Statistical analysis. For each of the variables tested, two-way analysis of variance (ANOVA) was used. A significant result was indicated by a p value < 0.05 (*) or by a p value < 0.01 (**). All the results are expressed as mean $\pm$ SD of triplicate determinations obtained in 3 independent experiments. Data were analyzed using the software GraphPad Prism 4.0 (GraphPad Software, Inc., La Jolla, CA).

Acknowledgements

The Authors wish to thank MIUR-PRIN for financial support.

Graphical Abstract

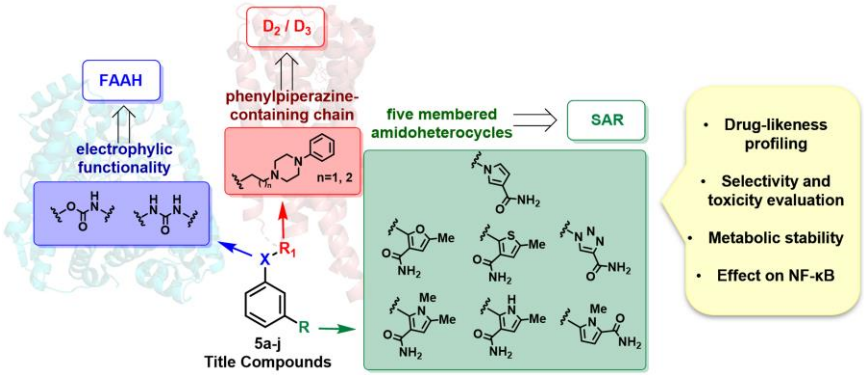

References

1. Lu, H. C.; Mackie, K., An Introduction to the Endogenous Cannabinoid System. *Biological psychiatry* **2016,** *79* (7), 516-25.
2. Castillo, P. E.; Younts, T. J.; Chavez, A. E.; Hashimotodani, Y., Endocannabinoid signaling and synaptic function. *Neuron* **2012,** *76* (1), 70-81.
3. Fernandez-Ruiz, J.; Hernandez, M.; Ramos, J. A., Cannabinoid-dopamine interaction in the pathophysiology and treatment of CNS disorders. *CNS neuroscience & therapeutics* **2010,** *16* (3), e72-91.
4. El Khoury, M. A.; Gorgievski, V.; Moutsimilli, L.; Giros, B.; Tzavara, E. T., Interactions between the cannabinoid and dopaminergic systems: evidence from animal studies. *Progress in neuro-psychopharmacology & biological psychiatry* **2012,** *38* (1), 36-50.
5. Garcia, C.; Palomo-Garo, C.; Gomez-Galvez, Y.; Fernandez-Ruiz, J., Cannabinoid-dopamine interactions in the physiology and physiopathology of the basal ganglia. *Br J Pharmacol* **2016,** *173* (13), 2069-79.
6. Knudsen, P.; Vilmar, T., Cannabis and neuroleptic agents in schizophrenia. *Acta psychiatrica Scandinavica* **1984,** *69* (2), 162-74.
7. Giuffrida, A.; Leweke, F. M.; Gerth, C. W.; Schreiber, D.; Koethe, D.; Faulhaber, J.; Klosterkotter, J.; Piomelli, D., Cerebrospinal anandamide levels are elevated in acute schizophrenia and are inversely correlated with psychotic symptoms. *Neuropsychopharmacology : official publication of the American College of Neuropsychopharmacology* **2004,** *29* (11), 2108-14.
8. Parsons, L. H.; Hurd, Y. L., Endocannabinoid signalling in reward and addiction. *Nat Rev Neurosci* **2015,** *16* (10), 579-94.
9. Solinas, M.; Justinova, Z.; Goldberg, S. R.; Tanda, G., Anandamide administration alone and after inhibition of fatty acid amide hydrolase (FAAH) increases dopamine levels in the nucleus accumbens shell in rats. *J Neurochem* **2006,** *98* (2), 408-19.
10. Scherma, M.; Panlilio, L. V.; Fadda, P.; Fattore, L.; Gamaleddin, I.; Le Foll, B.; Justinova, Z.; Mikics, E.; Haller, J.; Medalie, J.; Stroik, J.; Barnes, C.; Yasar, S.; Tanda, G.; Piomelli, D.; Fratta, W.; Goldberg, S. R., Inhibition of anandamide hydrolysis by cyclohexyl carbamic acid 3'-carbamoyl-3-yl ester (URB597) reverses abuse-related behavioral and neurochemical effects of nicotine in rats. *J Pharmacol Exp Ther* **2008,** *327* (2), 482-90.
11. Justinova, Z.; Panlilio, L. V.; Moreno-Sanz, G.; Redhi, G. H.; Auber, A.; Secci, M. E.; Mascia, P.; Bandiera, T.; Armirotti, A.; Bertorelli, R.; Chefer, S. I.; Barnes, C.; Yasar, S.; Piomelli, D.; Goldberg, S. R., Effects of Fatty Acid Amide Hydrolase (FAAH) Inhibitors in Non-Human Primate Models of Nicotine Reward and Relapse. *Neuropsychopharmacology : official publication of the American College of Neuropsychopharmacology* **2015,** *40* (9), 2185-97.
12. Cippitelli, A.; Astarita, G.; Duranti, A.; Caprioli, G.; Ubaldi, M.; Stopponi, S.; Kallupi, M.; Sagratini, G.; Rodriguez de Fonseca, F.; Piomelli, D.; Ciccocioppo, R., Endocannabinoid regulation

of acute and protracted nicotine withdrawal: effect of FAAH inhibition. *PloS one* **2011,** *6* (11), e28142.
13. https://www.who.int/news-room/fact-sheets/detail/tobacco (accessed 27/06/2019).
14. Butini, S.; Nikolic, K.; Kassel, S.; Bruckmann, H.; Filipic, S.; Agbaba, D.; Gemma, S.; Brogi, S.; Brindisi, M.; Campiani, G.; Stark, H., Polypharmacology of dopamine receptor ligands. *Progress in neurobiology* **2016,** *142*, 68-103.
15. https://clinicaltrials.gov/ct2/show/NCT01188967. (accessed 27/06/2019).
16. Okita, K.; Mandelkern, M. A.; London, E. D., Cigarette Use and Striatal Dopamine D2/3 Receptors: Possible Role in the Link between Smoking and Nicotine Dependence. *Int J Neuropsychopharmacol* **2016,** *19* (11).
17. De Simone, A.; Ruda, G. F.; Albani, C.; Tarozzo, G.; Bandiera, T.; Piomelli, D.; Cavalli, A.; Bottegoni, G., Applying a multitarget rational drug design strategy: the first set of modulators with potent and balanced activity toward dopamine D3 receptor and fatty acid amide hydrolase. *Chem Commun (Camb)* **2014,** *50* (38), 4904-7.
18. De Simone, A.; Russo, D.; Ruda, G. F.; Micoli, A.; Ferraro, M.; Di Martino, R. M.; Ottonello, G.; Summa, M.; Armirotti, A.; Bandiera, T.; Cavalli, A.; Bottegoni, G., Design, Synthesis, Structure-Activity Relationship Studies, and Three-Dimensional Quantitative Structure-Activity Relationship (3D-QSAR) Modeling of a Series of O-Biphenyl Carbamates as Dual Modulators of Dopamine D3 Receptor and Fatty Acid Amide Hydrolase. *J Med Chem* **2017,** *60* (6), 2287-2304.
19. Proschak, E.; Stark, H.; Merk, D., Polypharmacology by Design: A Medicinal Chemist's Perspective on Multitargeting Compounds. *J Med Chem* **2018**.
20. Campiani, G.; Butini, S.; Fattorusso, C.; Trotta, F.; Gemma, S.; Catalanotti, B.; Nacci, V.; Fiorini, I.; Cagnotto, A.; Mereghetti, I.; Mennini, T.; Minetti, P.; Di Cesare, M. A.; Stasi, M. A.; Di Serio, S.; Ghirardi, O.; Tinti, O.; Carminati, P., Novel atypical antipsychotic agents: rational design, an efficient palladium-catalyzed route, and pharmacological studies. *J Med Chem* **2005,** *48* (6), 1705-8.
21. Butini, S.; Gemma, S.; Campiani, G.; Franceschini, S.; Trotta, F.; Borriello, M.; Ceres, N.; Ros, S.; Coccone, S. S.; Bernetti, M.; De Angelis, M.; Brindisi, M.; Nacci, V.; Fiorini, I.; Novellino, E.; Cagnotto, A.; Mennini, T.; Sandager-Nielsen, K.; Andreasen, J. T.; Scheel-Kruger, J.; Mikkelsen, J. D.; Fattorusso, C., Discovery of a new class of potential multifunctional atypical antipsychotic agents targeting dopamine D3 and serotonin 5-HT1A and 5-HT2A receptors: design, synthesis, and effects on behavior. *J Med Chem* **2009,** *52* (1), 151-69.
22. Brindisi, M.; Butini, S.; Franceschini, S.; Brogi, S.; Trotta, F.; Ros, S.; Cagnotto, A.; Salmona, M.; Casagni, A.; Andreassi, M.; Saponara, S.; Gorelli, B.; Weikop, P.; Mikkelsen, J. D.; Scheel-Kruger, J.; Sandager-Nielsen, K.; Novellino, E.; Campiani, G.; Gemma, S., Targeting dopamine D3 and serotonin 5-HT1A and 5-HT2A receptors for developing effective antipsychotics: synthesis, biological characterization, and behavioral studies. *J Med Chem* **2014,** *57* (22), 9578-97.
23. Campiani, G.; Butini, S.; Trotta, F.; Fattorusso, C.; Catalanotti, B.; Aiello, F.; Gemma, S.; Nacci, V.; Novellino, E.; Stark, J. A.; Cagnotto, A.; Fumagalli, E.; Carnovali, F.; Cervo, L.; Mennini, T., Synthesis and pharmacological evaluation of potent and highly selective D3 receptor ligands: inhibition of cocaine-seeking behavior and the role of dopamine D3/D2 receptors. *J Med Chem* **2003,** *46* (18), 3822-39.
24. Butini, S.; Brindisi, M.; Gemma, S.; Minetti, P.; Cabri, W.; Gallo, G.; Vincenti, S.; Talamonti, E.; Borsini, F.; Caprioli, A.; Stasi, M. A.; Di Serio, S.; Ros, S.; Borrelli, G.; Maramai, S.; Fezza, F.; Campiani, G.; Maccarrone, M., Discovery of potent inhibitors of human and mouse fatty acid amide hydrolases. *J Med Chem* **2012,** *55* (15), 6898-915.
25. Butini, S.; Gemma, S.; Brindisi, M.; Maramai, S.; Minetti, P.; Celona, D.; Napolitano, R.; Borsini, F.; Cabri, W.; Fezza, F.; Merlini, L.; Dallavalle, S.; Campiani, G.; Maccarrone, M., Identification of a novel arylpiperazine scaffold for fatty acid amide hydrolase inhibition with improved drug disposition properties. *Bioorg Med Chem Lett* **2013,** *23* (2), 492-5.

26. Brindisi, M.; Borrelli, G.; Brogi, S.; Grillo, A.; Maramai, S.; Paolino, M.; Benedusi, M.; Pecorelli, A.; Valacchi, G.; Di Cesare Mannelli, L.; Ghelardini, C.; Allara, M.; Ligresti, A.; Minetti, P.; Campiani, G.; di Marzo, V.; Butini, S.; Gemma, S., Development of Potent Inhibitors of Fatty Acid Amide Hydrolase Useful for the Treatment of Neuropathic Pain. *ChemMedChem* **2018,** *13* (19), 2090-2103.
27. Brindisi, M.; Maramai, S.; Gemma, S.; Brogi, S.; Grillo, A.; Di Cesare Mannelli, L.; Gabellieri, E.; Lamponi, S.; Saponara, S.; Gorelli, B.; Tedesco, D.; Bonfiglio, T.; Landry, C.; Jung, K. M.; Armirotti, A.; Luongo, L.; Ligresti, A.; Piscitelli, F.; Bertucci, C.; Dehouck, M. P.; Campiani, G.; Maione, S.; Ghelardini, C.; Pittaluga, A.; Piomelli, D.; Di Marzo, V.; Butini, S., Development and Pharmacological Characterization of Selective Blockers of 2-Arachidonoyl Glycerol Degradation with Efficacy in Rodent Models of Multiple Sclerosis and Pain. *Journal of medicinal chemistry* **2016,** *59* (6), 2612-32.
28. Brindisi, M.; Brogi, S.; Maramai, S.; Grillo, A.; Borrelli, G.; Butini, S.; Novellino, E.; Allara, M.; Ligresti, A.; Campiani, G.; Di Marzo, V.; Gemma, S., Harnessing the pyrroloquinoxaline scaffold for FAAH and MAGL interaction: definition of the structural determinants for enzyme inhibition. *Rsc Adv* **2016,** *6* (69), 64651-64664.
29. Colangeli, R.; Pierucci, M.; Benigno, A.; Campiani, G.; Butini, S.; Di Giovanni, G., The FAAH inhibitor URB597 suppresses hippocampal maximal dentate afterdischarges and restores seizure-induced impairment of short and long-term synaptic plasticity. *Scientific reports* **2017,** *7* (1), 11152.
30. Lim, J.; Igarashi, M.; Jung, K. M.; Butini, S.; Campiani, G.; Piomelli, D., Endocannabinoid Modulation of Predator Stress-Induced Long-Term Anxiety in Rats. *Neuropsychopharmacology : official publication of the American College of Neuropsychopharmacology* **2016,** *41* (5), 1329-39.
31. Basso, E.; Duranti, A.; Mor, M.; Piomelli, D.; Tontini, A.; Tarzia, G.; Traldi, P., Tandem mass spectrometric data-FAAH inhibitory activity relationships of some carbamic acid O-aryl esters. *Journal of mass spectrometry : JMS* **2004,** *39* (12), 1450-5.
32. Alexander, J. P.; Cravatt, B. F., Mechanism of carbamate inactivation of FAAH: implications for the design of covalent inhibitors and in vivo functional probes for enzymes. *Chemistry & biology* **2005,** *12* (11), 1179-87.
33. Boger, D. L.; Miyauchi, H.; Du, W.; Hardouin, C.; Fecik, R. A.; Cheng, H.; Hwang, I.; Hedrick, M. P.; Leung, D.; Acevedo, O.; Guimaraes, C. R.; Jorgensen, W. L.; Cravatt, B. F., Discovery of a potent, selective, and efficacious class of reversible alpha-ketoheterocycle inhibitors of fatty acid amide hydrolase effective as analgesics. *J Med Chem* **2005,** *48* (6), 1849-56.
34. Khatri, M.; Rai, S. K.; Ranbhor, R.; Kishore, K.; Tiwari, M., Synthesis and pharmacological evaluation of [(4-arylpiperazin-1-yl)-alkyl]-carbamic acid ethyl ester derivatives as potential anxiolytic agents. *Arch Pharm Res* **2012,** *35* (7), 1143-52.
35. De, S. K., Sulfamic acid as a novel, efficient, cost-effective, and reusable solid acid catalyst for the synthesis of pyrroles under solvent-free conditions. *Synthetic Commun* **2008,** *38* (5), 803-809.
36. Zhu, W.; Ma, D. W., Synthesis of aryl azides and vinyl azides via proline-promoted CuI-catalyzed coupling reactions. *Chem Commun* **2004,** (7), 888-889.
37. Himo, F.; Lovell, T.; Hilgraf, R.; Rostovtsev, V. V.; Noodleman, L.; Sharpless, K. B.; Fokin, V. V., Copper(I)-catalyzed synthesis of azoles. DFT study predicts unprecedented reactivity and intermediates. *J Am Chem Soc* **2005,** *127* (1), 210-6.
38. Gemma, S.; Camodeca, C.; Brindisi, M.; Brogi, S.; Kukreja, G.; Kunjir, S.; Gabellieri, E.; Lucantoni, L.; Habluetzel, A.; Taramelli, D.; Basilico, N.; Gualdani, R.; Tadini-Buoninsegni, F.; Bartolommei, G.; Moncelli, M. R.; Martin, R. E.; Summers, R. L.; Lamponi, S.; Savini, L.; Fiorini, I.; Valoti, M.; Novellino, E.; Campiani, G.; Butini, S., Mimicking the intramolecular hydrogen bond: synthesis, biological evaluation, and molecular modeling of benzoxazines and quinazolines as potential antimalarial agents. *Journal of medicinal chemistry* **2012,** *55* (23), 10387-404.

39. Gemma, S.; Camodeca, C.; Sanna Coccone, S.; Joshi, B. P.; Bernetti, M.; Moretti, V.; Brogi, S.; Bonache de Marcos, M. C.; Savini, L.; Taramelli, D.; Basilico, N.; Parapini, S.; Rottmann, M.; Brun, R.; Lamponi, S.; Caccia, S.; Guiso, G.; Summers, R. L.; Martin, R. E.; Saponara, S.; Gorelli, B.; Novellino, E.; Campiani, G.; Butini, S., Optimization of 4-aminoquinoline/clotrimazole-based hybrid antimalarials: further structure-activity relationships, in vivo studies, and preliminary toxicity profiling. *J Med Chem* **2012,** *55* (15), 6948-67.
40. Sirous, H.; Fassihi, A.; Brogi, S.; Campiani, G.; Christ, F.; Debyser, Z.; Gemma, S.; Butini, S.; Chemi, G.; Grillo, A.; Zabihollahi, R.; Aghasadeghi, M. R.; Saghaie, L.; Memarian, H. R., Synthesis, Molecular Modelling and Biological Studies of 3-hydroxy-pyrane-4-one and 3-hydroxy-pyridine-4-one Derivatives as HIV-1 Integrase Inhibitors. *Med Chem* **2018**.
41. Iwatsubo, T.; Hirota, N.; Ooie, T.; Suzuki, H.; Shimada, N.; Chiba, K.; Ishizaki, T.; Green, C. E.; Tyson, C. A.; Sugiyama, Y., Prediction of in vivo drug metabolism in the human liver from in vitro metabolism data. *Pharmacology & therapeutics* **1997,** *73* (2), 147-71.
42. Biala, G.; Pekala, K.; Boguszewska-Czubara, A.; Michalak, A.; Kruk-Slomka, M.; Grot, K.; Budzynska, B., Behavioral and Biochemical Impact of Chronic Unpredictable Mild Stress on the Acquisition of Nicotine Conditioned Place Preference in Rats. *Molecular neurobiology* **2018,** *55* (4), 3270-3289.
43. Vargas, H. O.; Nunes, S. O.; de Castro, M. R.; Vargas, M. M.; Barbosa, D. S.; Bortolasci, C. C.; Venugopal, K.; Dodd, S.; Berk, M., Oxidative stress and inflammatory markers are associated with depression and nicotine dependence. *Neuroscience letters* **2013,** *544*, 136-40.
44. Newman, M. B.; Arendash, G. W.; Shytle, R. D.; Bickford, P. C.; Tighe, T.; Sanberg, P. R., Nicotine's oxidative and antioxidant properties in CNS. *Life sciences* **2002,** *71* (24), 2807-20.
45. Budzynska, B.; Boguszewska-Czubara, A.; Kruk-Slomka, M.; Skalicka-Wozniak, K.; Michalak, A.; Musik, I.; Biala, G.; Glowniak, K., Effects of imperatorin on nicotine-induced anxiety- and memory-related responses and oxidative stress in mice. *Physiology & behavior* **2013,** *122*, 46-55.
46. Nunes, S. O.; Vargas, H. O.; Prado, E.; Barbosa, D. S.; de Melo, L. P.; Moylan, S.; Dodd, S.; Berk, M., The shared role of oxidative stress and inflammation in major depressive disorder and nicotine dependence. *Neuroscience and biobehavioral reviews* **2013,** *37* (8), 1336-45.
47. Chung, S.; Sundar, I. K.; Hwang, J. W.; Yull, F. E.; Blackwell, T. S.; Kinnula, V. L.; Bulger, M.; Yao, H.; Rahman, I., NF-kappaB inducing kinase, NIK mediates cigarette smoke/TNFalpha-induced histone acetylation and inflammation through differential activation of IKKs. *PloS one* **2011,** *6* (8), e23488.
48. Swan, G. E.; Lessov-Schlaggar, C. N., The effects of tobacco smoke and nicotine on cognition and the brain. *Neuropsychology review* **2007,** *17* (3), 259-73.
49. Gasser, A.; Brogi, S.; Urayama, K.; Nishi, T.; Kurose, H.; Tafi, A.; Ribeiro, N.; Desaubry, L.; Nebigil, C. G., Discovery and cardioprotective effects of the first non-Peptide agonists of the G protein-coupled prokineticin receptor-1. *PloS one* **2015,** *10* (4), e0121027.
50. Mileni, M.; Garfunkle, J.; Ezzili, C.; Cravatt, B. F.; Stevens, R. C.; Boger, D. L., Fluoride-mediated capture of a noncovalent bound state of a reversible covalent enzyme inhibitor: X-ray crystallographic analysis of an exceptionally potent alpha-ketoheterocycle inhibitor of fatty acid amide hydrolase. *J Am Chem Soc* **2011,** *133* (11), 4092-100.
51. Wang, S.; Che, T.; Levit, A.; Shoichet, B. K.; Wacker, D.; Roth, B. L., Structure of the D2 dopamine receptor bound to the atypical antipsychotic drug risperidone. *Nature* **2018,** *555* (7695), 269-273.
52. Chien, E. Y.; Liu, W.; Zhao, Q.; Katritch, V.; Han, G. W.; Hanson, M. A.; Shi, L.; Newman, A. H.; Javitch, J. A.; Cherezov, V.; Stevens, R. C., Structure of the human dopamine D3 receptor in complex with a D2/D3 selective antagonist. *Science* **2010,** *330* (6007), 1091-5.
53. Brogi, S.; Fiorillo, A.; Chemi, G.; Butini, S.; Lalle, M.; Ilari, A.; Gemma, S.; Campiani, G., Structural characterization of Giardia duodenalis thioredoxin reductase (gTrxR) and computational analysis of its interaction with NBDHEX. *Eur J Med Chem* **2017,** *135*, 479-490.

54. Chemi, G.; Gemma, S.; Campiani, G.; Brogi, S.; Butini, S.; Brindisi, M., Computational Tool for Fast in silico Evaluation of hERG K(+) Channel Affinity. *Front Chem* **2017,** *5*, 7.
55. Friesner, R. A.; Banks, J. L.; Murphy, R. B.; Halgren, T. A.; Klicic, J. J.; Mainz, D. T.; Repasky, M. P.; Knoll, E. H.; Shelley, M.; Perry, J. K.; Shaw, D. E.; Francis, P.; Shenkin, P. S., Glide: a new approach for rapid, accurate docking and scoring. 1. Method and assessment of docking accuracy. *J Med Chem* **2004,** *47* (7), 1739-49.
56. Fezza, F.; Marrone, M. C.; Avvisati, R.; Di Tommaso, M.; Lanuti, M.; Rapino, C.; Mercuri, N. B.; Maccarrone, M.; Marinelli, S., Distinct modulation of the endocannabinoid system upon kainic acid-induced in vivo seizures and in vitro epileptiform bursting. *Molecular and cellular neurosciences* **2014,** *62*, 1-9.
57. Lamponi, S.; Aloisi, A. M.; Bonechi, C.; Consumi, M.; Donati, A.; Leone, G.; Rossi, C.; Tamasi, G.; Ghiandai, L.; Ferrini, E.; Fiorenzani, P.; Ceccarelli, I.; Magnani, A., Evaluation of in vitro cell and blood compatibility and in vivo analgesic activity of plant-derived dietary supplements. *Journal of integrative medicine* **2019,** *17* (3), 213-220.
58. D'Elia, P.; De Matteis, F.; Dragoni, S.; Shah, A.; Sgaragli, G.; Valoti, M., DP7, a novel dihydropyridine multidrug resistance reverter, shows only weak inhibitory activity on human CYP3A enzyme(s). *Eur J Pharmacol* **2009,** *614* (1-3), 7-13.
59. Williamson, B.; Wilson, C.; Dagnell, G.; Riley, R. J., Harmonised high throughput microsomal stability assay. *Journal of pharmacological and toxicological methods* **2017,** *84*, 31-36.
60. Brogi, S.; Ramunno, A.; Savi, L.; Chemi, G.; Alfano, G.; Pecorelli, A.; Pambianchi, E.; Galatello, P.; Compagnoni, G.; Focher, F.; Biamonti, G.; Valacchi, G.; Butini, S.; Gemma, S.; Campiani, G.; Brindisi, M., First dual AK/GSK-3beta inhibitors endowed with antioxidant properties as multifunctional, potential neuroprotective agents. *Eur J Med Chem* **2017,** *138*, 438-457.
61. Cavicchio, C.; Benedusi, M.; Pambianchi, E.; Pecorelli, A.; Cervellati, F.; Savelli, V.; Calamandrei, D.; Maellaro, E.; Rispoli, G.; Maioli, E.; Valacchi, G., Potassium Ascorbate with Ribose: Promising Therapeutic Approach for Melanoma Treatment. *Oxidative medicine and cellular longevity* **2017,** *2017*, 4256519.
62. Canella, R.; Benedusi, M.; Martini, M.; Cervellati, F.; Cavicchio, C.; Valacchi, G., Role of Nrf2 in preventing oxidative stress induced chloride current alteration in human lung cells. *Journal of cellular physiology* **2018,** *233* (8), 6018-6027.